Advances in Applied Energy 2 (2021) 100028

Contents lists available at ScienceDirect

Advances in Applied Energy

journal homepage: www.elsevier.com/locate/adapen

Development and experimental validation of hierarchical energy management system based on stochastic model predictive control for Off-grid Microgrids

Simone Polimeni [a,*], Lorenzo Meraldi [a,b], Luca Moretti [a], Sonia Leva [a], Giampaolo Manzolini [a]

[a] Politecnico di Milano, Dipartimento di Energia, Via Lambruschini 4, 20156, Milano, Italy
[b] Engie EPS, Via Grazzini 14, 20159, Milano, Italy

ARTICLE INFO

Keywords:
Energy management systems
Off-grid Microgrid
Stochastic model predictive control
MILP optimization

ABSTRACT

In this study, a hierarchical energy management system (EMS) is proposed, to coordinate different energy sources in an islanded multi-good microgrid. The first layer deals with the daily scheduling problem, while the second layer balances the generation in real-time. A novel second layer formulation, relying on model predictive control under a scenario-based stochastic approach (sMPC), is introduced and it is compared to a reference formulation, based on a central proportional-integral controller following the indications set by the first layer. The proposed sMPC explicitly accounts for uncertainty considering several scenarios of very-short term forecast errors, that act as disturbances for the system. The sMPC evaluates the control actions and the correction rules required to guarantee optimal operations through disturbance-feedback. The EMS is implemented in an experimental setup and tested for daily operations under a rolling horizon approach. The accuracy of the numerical system simulation is evaluated, resulting in an average discrepancy of 1.7%, in terms of operation cost, with respect to the experimental operations. Then, a test case comparing the proposed EMS with the reference approach shows that the adoption of sMPC allows to approach the lowest possible operation cost achievable by a second layer with an advantage of 2.7 % against the reference case. Finally, the developed sMPC leads to only 0.5% additional costs than an ideal controller working on the same control layer.

Indices

i	General microgrid unit
g	Generator
g_f	Fossil fueled generator
g_{gd}^{pr}	Generator producing good gd
g_{gd}^{cn}	Generator consuming good gd
s	Storage system
s^{NS}	Storage system with non-simultaneous charge and discharge behavior
s_{gd}	Storage system participating in good gd balance
gd	Microgrid good
cu	Curtailment (fictitious unit)
um	Unmet good demand (fictitious unit)
t	First-layer timestep
k	Second-layer timestep
Δt	Absolute time between consecutive timesteps (first layer)
$\Delta t'$	Absolute time between consecutive timesteps (second layer)
sc	Scenario in stochastic problem

Parameters

$\hat{D}^{gd}$	Forecasted value of net demand of good gd
$\tilde{D}^{gd}$	Realization of net demand of good gd
$\bar{D}^{gd}$	Nominal forecasted value of net demand of good gd
$\hat{\xi}^{gd}$	Forecast error estimation
$\tilde{\xi}^{gd}$	Realization of forecast error
π_{sc}	Probability of scenario sc
N_{sc}	Number of real-time scenarios
$\hat{C}^s_{min}, \hat{C}^s_{max}$	Minimum and maximum levels of storage s
$\hat{\eta}^s_{ch}, \hat{\eta}^s_{dh}$	Charging and discharging efficiency of storage system s
$\hat{L}^s$	Good losses in the storage system s (hourly losses)
$\hat{U}^i_{min}, \hat{U}^i_{max}$	Minimum and maximum set-point of unit i
$\widehat{\Delta U}^i_{UP}, \widehat{\Delta U}^i_{DW}$	Ramp up and ramp down limit of unit i (hourly ramp)
$\widehat{\Delta U}^g_{max,SU}$, $\Delta\hat{U}^g_{max,SD}$	Maximum set-point variation of generator g during start-up and shut-down

* Corresponding author.
E-mail address: simone.polimeni@polimi.it (S. Polimeni).

https://doi.org/10.1016/j.adapen.2021.100028
Received 19 April 2021; Received in revised form 26 April 2021; Accepted 27 April 2021
Available online 4 May 2021

$\widehat{UT}^g, \widehat{DT}^g$	Minimum up-time and down-time for generator g
$\boldsymbol{A}^i, \boldsymbol{B}^i, \boldsymbol{C}^i, \boldsymbol{D}^i$	State space matrixes of unit i, dynamic representation with time resolution $\Delta t'$
$\hat{\chi}^{i,gd}$	Parameter to identify participation of unit i in the balance of good gd
$\hat{m}_t^i$, $\hat{q}_t^i$	Generic coefficients for linear formulation for unit i
$\hat{k}$	Generic cost coefficient
$\hat{\sigma}$	Upper storage state of charge flag

Variables First layer

Z_t^g	Commitment status of generator g,
SU_t^g, SD_t^g	Start-up and shut-down decisions of generator g
I_t^g, U_t^g	Consumption and production of generator g
C_t^s	Level of storage s
U_t^s	Bus balance for storage s
$U_t^{s,ch}, U_t^{s,dh}$	Charging and discharging power for storage s
Z_t^s	Binary variable for storage charge/discharge decision (if required)
UM_t^{gd}, CU_t^{gd}	Unmet demand and curtailment for good gd
$\Delta_t^{SOC,gd}$	SOC deviation among different storages participating in the same good balance

Second layer

u_k^i	Set-point to unit i
$\delta u_t^i(\xi^{gd})$	Set-point correction to unit i
x_t^i	State vector of unit i
y_t^i	Output vector of unit i
$f_t^{g_f}$	Fuel consumption of generator g_f
z_t^i, Aux_t^i	Generic auxiliary variables, $z_t^i \in \{0,1\}$, $Aux_t^i \in \mathbb{R}$

1. Introduction

The microgrid (MG) concept has received large attention over the past few years, offering a successful approach to integrate distributed renewable energy sources (RES) with local loads. A typical MG configuration includes RES, energy storage systems (ESS), and dispatchable generators (DG), representing a small-scale power system [1]. Multi-goods microgrids (MGMG) or multi-energy systems (MES) represent an extension of this concept, handling the management of different energy forms to satisfy energy-related services (e.g. electricity, heating, cooling, and energy-dependent production processes) [2]; for instance, the successful integration of different services for an industrial consumer was demonstrated in [3], in terms of both emissions and cost reduction. A large penetration of RES leads to relevant challenges in operating the MG units in a synergic way, due to the intermittent and uncertain nature of RES power generation (i.e. solar and wind energy), that hinders the perfect exploitation of the available natural resources. Many researchers have focused on the development of intelligent energy management systems (EMS), to provide cost-effective solutions that ensure reliable operation and minimum environmental impact [4]. A comprehensive EMS must be designed to respect the control hierarchy required by such systems, usually including up to three levels of control [5]. Indeed, the challenge posed by the MG paradigm concerns issues at different time scales, ranging from primary control for voltage and frequency regulation to scheduling decisions [6]. For these reasons, the EMS is usually designed with a multi-layer structure: the first layer is in charge of the medium-term operation schedule (usually dealing with the operating strategy for the following 24 hours), while the second layer deals with the real-time balancing of the system; nevertheless, single-layer EMS have also been discussed in literature [7]. The evaluation of the optimal operation schedule consists in the evaluation of the most effective unit commitment (UC) of the controllable generators and loads, together with the economic dispatch (ED) of all the MG subsystems, exploiting the forecasts of the various internal consumption profiles and RES generation, while providing enough flexibility and reserve margins, to compensate for forecast errors, occurring in real-time operations [8]. A variety of solutions for predictive EMS algorithms has been proposed in the literature. The most commonly adopted framework is represented by mixed-integer linear problem (MILP) formulations, which identify the global optimal solution, but require a sufficiently accurate linearized model of the system [9]. Due to the high uncertainty of the forecasts, upon which the predictive optimization is based, the formulation of deterministic MILP must account for power reserve of the programmable generators, to ensure security-constrained ED [10]. Spinning reserve constraints sometimes lead to conservative or unfeasible solutions, if the reserve margins are not set correctly [11]. To overcome this issue, stochastic and robust approaches, which explicitly account for forecasts' uncertainty, have been widely used and validated as EMS in several applications [12, 13]. Stochastic models usually rely on a two-stage formulation, where the second-stage variables are scenario dependent, while the first-stage ones are common to all the scenarios. The aim of the optimization is to minimize the first-stage cost and the expected cost of recourse (related to the second-stage decisions), while achieving a feasible solution in all the considered scenarios [14]. Robust optimization algorithms are based on the definition of an uncertainty set, that ensure the feasibility of the solution for all the potential realization of the uncertain parameters [15]. Moretti et al. in [16] demonstrated the increase of service reliability achieved by the day-ahead robust UC with respect to the deterministic one, for MGMG both on-grid and off-grid configurations. In [17], the robustness of the stochastic UC formulation was improved by accounting for worst-case scenarios, which are iteratively added to the main problem Results show that efficient solutions are achieved both in terms of expected and worst-case cost. An hybrid robust-stochastic approach was introduced in [18]to optimize the market participation of a MG with RES and micro-turbines accounting for uncertainty of market prices, load and RES generation. Furthermore, a detailed comparison among deterministic, stochastic and robust formulations as EMS for microgrids has been carried out in [19], highlighting the fact that stochastic policies perform better in terms of total cost. In general, the pervasive employment of RES, combined with the aleatory load demand, brings about a large uncertainty of the power production requirements by the programmable MG units and storage systems, that may prevent the maximum exploitation renewable power generation (Figure 1). An EMS must consider the uncertain and stochastic behavior of net load demand, to compensate for its unpredicted variations, also at different time scales. Stochastic optimization applied to power management control problems has been recognized as an useful tool to obtain interesting results in terms of reduction of operation cost, RES integration and storage management [20].

The purpose of this paper is to introduce a novel stochastic formulation to improve the performances of the two-layer hierarchical EMS presented in previous works [21, 22]. The first layer is based on deterministic optimization to solve the optimal UC, evaluating the operation scheduling of the MG according to a rolling horizon approach and dealing indirectly with forecast uncertainty through the enforcement of spinning reserve requirements. In the previous work, the second layer was based on heuristic rules and proportional-integral (PI) control for the real time balance of the MG. This work focuses on the adoption of stochastic control systems as second layer of the EMS to evaluate the advantages that can be obtained enhancing the real-time dispatch of the MG. The employment of stochastic programming to solve an optimal control problem is named stochastic Model Predictive Control (sMPC) [23]. In this context, the presence of uncertainty requires the implementation of *closed-loop* instead of *open-loop* policies: therefore, a state-feedback controller or a disturbance-feedback controller should be applied [24]. A single-layer EMS based on sMPC is introduced in [25] showing the operating cost reduction of an islanded MG. In [26], a comparison among three different formulation of sMPC is considered. The models are tested on a laboratory-scale MG, made of a battery bank,

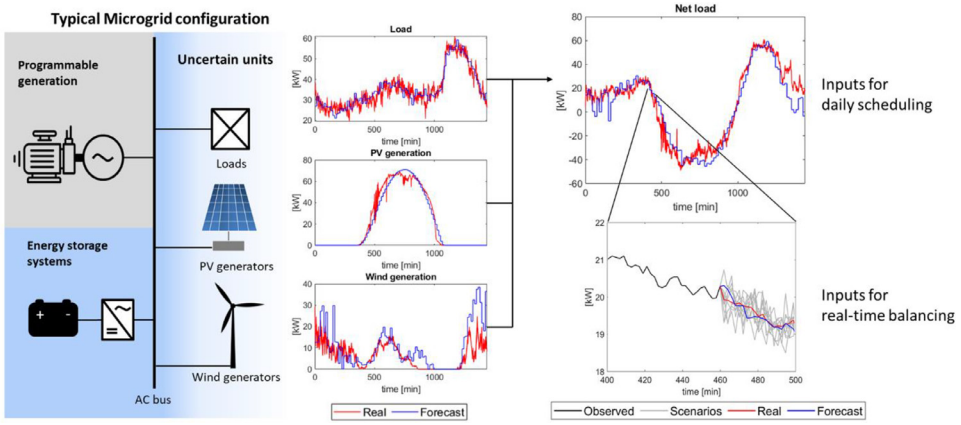

Fig. 1. Example of typical Microgrid configuration with uncertainty sources.

a fuel cell, an electrolyzer, hydrogen storage, and electric loads, in grid-connected mode. The authors showed that the scenario-based MPC is useful if there is a high availability of historical data, and it can guarantee a high level of demand satisfaction. An upper layer MPC is coupled with a rule-based real-time controller in [27], to ensure the optimal use of PV, BESS, and programmable appliances of a home microgrid. In [28], the idea of hierarchical control is applied to a large-scale PV microgrid, with both levels formulated as MPC problems, demonstrating the effectiveness of the approach both in numerical and hardware-in-the-loop simulations. A two-layer structure for the EMS is implemented in [29] to manage an on-grid microgrid composed of a microturbine, BESS, and PV. While the first layer optimizes the daily usage of the BESS and defines an energy exchange schedule with the main grid, the second layer aims to minimize the discrepancies with the schedule. Other works proved the effectiveness of sMPC approaches, demonstrating the advantages of its implementation both at higher optimization level and at lower control level. Improved control performances by a hierarchical sMPC over deterministic approach are mentioned in [30], for the management of electric vehicles in the context of a MG with wind uncertainty. Other sMPC strategies are implemented in [31,32] together with a scenario reduction method to reduce the computational burden of the stochastic controller. In both works, the proposed sMPC allowed a reduction of operation cost with respect to standard MPC approaches. Time decomposition strategies can also be considered to reduce the complexity of the optimization problem [33]. Even though there is a wide variety of EMS in literature, most of them are only validated through numerical simulations, whereas an experimental validation is mandatory to prove the physical soundness of the mathematical representation and the actual competitiveness of the proposed EMS architecture. Some experimental activities have been carried out for on-grid applications based on rule-based management [34], genetic algorithms [35], and MPC [36]. A two-layer EMS, with a MILP-based economic dispatch and a rule-based real-time controller, was developed and tested for a small grid-connected PV–BESS system, ensuring superior economic performances compared to a peak-shaving rule-based strategy [37]. Other works [26, 38] resort to an experimental on-grid MG to test the proposed EMS adopting stochastic optimization approaches, but they do not quantify the discrepancies between the EMS simulations and the actual operating profiles. In work [39], besides proposing an optimization model, a strong focus on battery efficiency is presented, highlighting the differences among three battery models: a constant efficiency model, and two models with variable efficiency depending on the input/output currents respectively in a linear and quadratic form. An optimization-based online EMS architecture has been proposed and experimentally tested in [40], considering a laboratory-scale microgrid comprising of one BESS, simulated PV and wind power generation, a load, and a grid connection: the experiments' time-frame is scaled down from hours to minutes, the online optimization model successfully manages the microgrid with reduced operation costs, but the differences between scheduling and control levels are not addressed, as no hierarchical structure is implemented.

The main contributions of this paper regard:

1 A novel formulation of the sMPC for real-time dispatch, that provides optimal set-points and correction rules to the MG units. Those correction rules are evaluated as first-stage variables independent from the particular scenarios considered during the optimization and directly employed to balance the MG production in real-time. The model relies on piecewise affine disturbance-feedback, considering as disturbances the future forecast errors of the net demands (*i.e.,* loads minus non dispatchable production). The formulation accounts for uncertainty of one or more demands and can be extended to complex MG configurations.
2 The implementation of the hierarchical EMS on an experimental facility, the Multi-Good MicroGrid Laboratory (MG^2Lab) [41]. Experimental activities are carried out to demonstrate the successful deployment of the EMS for off-grid systems and to validate the results that are obtained by the corresponding numerical simulation.

This paper is organized as follows. Section 2 describes the hierarchical EMS and provides the mathematical formulation of the novel sMPC. Section 3 provides details on the implementation of the EMS on the experimental facility and its architecture for on-line applications, while section 4 Shows the validation of the numerical results with experimental data for different days of operation. After the validation, a comparison between the proposed EMS and several benchmarks is presented in section 5, for an off-grid MGMG, providing potable water and electricity. In the paper, the first-layer variables are indicated with capital letters, the second-layer variables with lowercase letters. In addition, the parameters are expressed as $\hat{.}$, the values of the variables corresponding to the solution of the optimization problems as $\tilde{.}$, and the measurements or the realization of uncertain parameters with $\bar{.}$.

2. Energy management System description

The hierarchical EMS developed in this work is designed for the optimal management of single-bus islanded MGMGs. The description of the EMS is schematized in Figure 2. The first layer adopts a deterministic MILP formulation of the optimal scheduling problem, determining the UC and tentative ED plans that minimize the operating cost, based on the expected forecasts of demand and renewable generation. Reserve constraints ensure operating margins for real-time corrections to the scheduling plan defined in the first-layer, taken as a reference by the second layer. The optimization is periodically updated according to the rolling horizon approach, suitable for online applications [42]. The commitment status determined by the first layer is not modified during the advancement period: the second layer is therefore in charge of

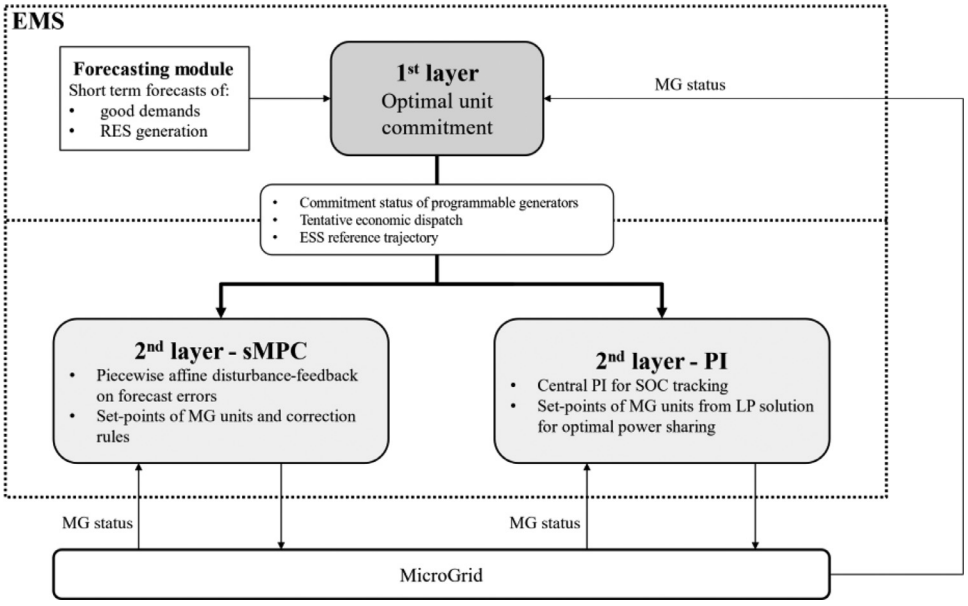

Fig. 2. Hierarchical EMS architecture.

adjusting the set-points of the committed units, to guarantee safe operation and competitive economic performance. Regardless of the algorithm adopted in the second-layer of the EMS, the conceptual structure remains the same. A scenario-based sMPC formulation for the second-layer controller is presented in the following section, to track the ESS state of charge (SOC) reference trajectory throughout the day modulating the total power output from the dispatchable generators, accounting for very short-term uncertainty of MG demands end RES generation. The proposed formulation is an alternative to the non-predictive second layer considered in a previous work [21]. The two alternative EMS are identified respectively as EMS_{sMPC} and EMS_{PI}, according to the second-layer control strategy adopted. A bottom layer that handles the control of electrical variables is not considered in this architecture, as it will be directly implemented in the local controllers of the MG units. The complete EMS must also include a forecast generation module, to provide the inputs required by the optimization model, as well as a feedback loop with the MG, to read the status of the units. The next paragraphs explain in detail the concept behind first and second layer, focusing on the sMPC formulation.

2.1. First-layer model

The model employed in this work was introduced in [21]. The objective function consists in the minimization of the microgrid operating cost, namely (i) fuel consumption, (ii) start-up cost of programmable units, (iii) wearing cost of storage systems and generators and (iv) penalization for unmet critical demands as well as curtailment of RES generation. The operating space of the dispatchable generators is defined by their technical limits, including minimum/maximum load, minimum up/downtime, and ramping limitations. The storage systems are constrained by their minimum and maximum capacity, and by their maximum capability of exchanging stored goods with the MG. As [21] considers only one BESS, a slight variation on the objective function has been introduced in this model. Indeed, when considering several identical BESS, the MILP solver does not show any preference in their dispatch, as long as all the related constraints are not violated. Therefore, a penalization was introduced, to minimize the deviation of the SOC of all the identical BESS which participate to the balance of the same good. Moreover, to improve the repeatability of the simulation, the cost coefficients related to controllable generators and the curtailment are set as decreasing time-varying parameter; this artifice allows to reduce the number of equivalent solutions when solving the optimization problem. The mathematical formulation of the first-layer layer model is detailed in appendix A.

2.2. Second-layer model of EMS_{sMPC}

According to the hierarchical control structure of the EMS, the purpose of the second layer is to track the first-layer reference dispatch plan as closely as possible, while defining the unavoidable deviations mainly related to forecast errors (uncertain demands, wind and PV generations). For linear systems, the general MPC formulation for tracking of reference signals takes the following form [43, 44]:

$$\min J = \sum_{k=1}^{H} \|u_k - \bar{U}_k\|_Q^2 + \|x_k - \bar{X}_k\|_Q^2; \tag{1}$$

s.t.

$$x_{k+1} = \boldsymbol{A}x_k + \boldsymbol{B}u_k + \boldsymbol{M}d_k \tag{2}$$

$$y_{k+1} = \boldsymbol{C}x_k + \boldsymbol{D}u_k \tag{3}$$

Due to the uncertain nature of the control problem, a deterministic approach is not suitable for the second layer. As suggested by [29], the employment of a stochastic approach at the lower-layer is beneficial and efficient for MG management. Therefore, an sMPC with disturbance-feedback based on scenarios of forecast errors is proposed. The disturbances are identified as the forecast errors of the net demands, with respect to the predictions considered by the first layer. The second layer optimizes the power sharing among the MG units, and it does not modify the commitment status of the programmable generators, only set and updated by the first layer. Some features of the model and of typical MG units (*i.e.,* piecewise formulations), make it necessary to include logical conditions and auxiliary binary variables in the MPC model, that makes it no longer linear. This holds true especially if a correct characterization of the BESS is foreseen as simultaneous charge and discharge are not allowed, and the two operations are characterized by different efficiencies. To overcome this issue, authors in [29] defined two separate problems, to be solved in parallel: one imposing only BESS charge and the other one only discharge along the optimization horizon. The actual BESS set-point is decided *a posteriori*, checking which problem has the lowest objective function; then, it is applied for the first time-step and the two models are solved again, following the rolling horizon approach. In work [25], an sMPC formulation is proposed, with a disturbance-feedback approach with fixed recourse coefficients, and employing a

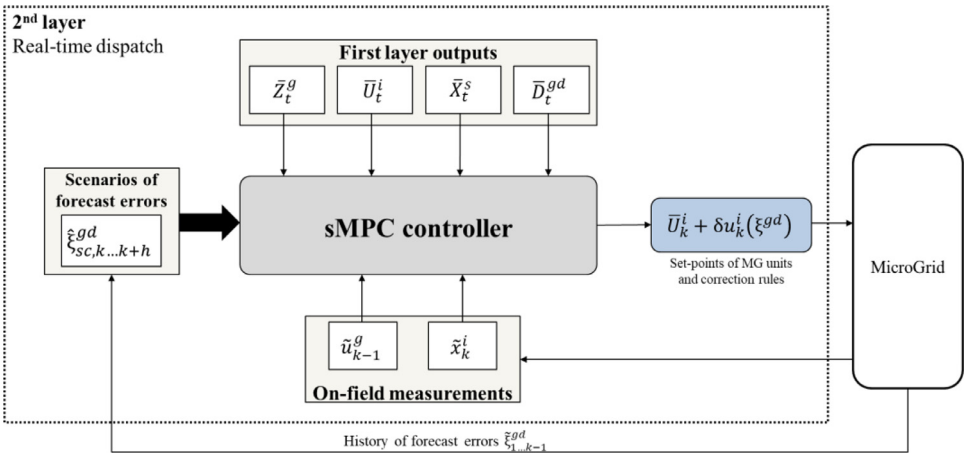

Fig. 3. EMS second layer flowchart for sMPC.

simplified formulation for the storage system. The proposed sMPC considers an accurate description of the storage system while computing the optimal affine policies that define the power-sharing among the units of the microgrid as a function of the future forecast errors. To explicitly account for the uncertainty, the formulation relies on variable recourse coefficients to define the affine laws under a disturbance-feedback approach (see eq (12)). Those policies will be used in real-time to adjust the set-points of the units. The detailed model is presented in the next sections, while Figure 3 shows the conceptual scheme of the second-layer formulation.

2.2.1. Objective function

In the stochastic framework, the objective is to minimize the expected cost among a set of scenarios; therefore, the objective function is written according to eq. (4):

$$\min J = \sum_{sc=1}^{N} \pi_{sc}\ J_{sc}; \tag{4}$$

The objective function commonly adopted in MPC formulations includes the norms which represent the tracking of the reference signals (both in terms of state and control variables). The mathematical expression of the objective function for each scenario is shown in eq. (5), comprising tracking cost $c_{st,k}^{Track}$, fuel cost $c_{g_f,k}^{f}$, unmet demand cost $c_{gd,k}^{UM}$ and curtailment cost $c_{gd,k}^{Curt}$:

$$J_{sc} = \sum_{k=1}^{T'} \left[\sum_{i} c_{i,k}^{track} + \sum_{s} c_{s,k}^{track,SOC} + \sum_{g_f} c_{g_f,k}^{f} + \sum_{gd} c_{gd,k}^{UM} + \sum_{gd} c_{gd,k}^{Curt} \right] \Delta t' \Big|_{sc}; \tag{5}$$

Where:

$$c_{i,k}^{track} = \left\| u_{i,k} - \bar{U}_{i,t} \right\|_{Q}^{2}; \tag{6}$$

$$c_{s,k}^{track,SOC} \geq \begin{cases} K\ \left(\bar{C}_{s,t} - x_k^s\right); \\ 0. \end{cases} \tag{7}$$

$$c_{g_f,k}^{f} = \hat{k}_f f_{sc,k}^{g_f};\ \ c_{gd,k}^{UM} = \hat{k}_{um} y_{sc,k}^{um};\ c_{gd,k}^{CU} = \hat{k}_{cu} y_{sc,k}^{cu}; \tag{8}$$

In particular, $c_{i,k}^{track}$ represents the tracking cost on the control signal with respect to the set-point computed by the first layer. The cost for tracking the state of the system has been neglected for all the programmable generators. Indeed, no state reference is retrieved for these components by the first layer with the exception of the unmodifiable commitment status, as the first layer does not account for the dynamic response of those units due to its coarse time discretization. On the contrary, tracking the state of the ESS is a very crucial task, to guarantee that the reserve margins imposed by the first layer are satisfied. While there is an interest in keeping the SOC as close as possible to the predicted value, higher SOC values do not affect the reliability of the MG operation, while the economic competitiveness is ensured by the other components of the objective function (*i.e.,* the ESS will only be charged to a higher SOC than the reference only if the RES generation was underestimated in the first layer, but not by controllable generators). For this reason, the correspondent cost $c_{s,k}^{track,SOC}$ has a piecewise behavior to reflect the asymmetric requirement for the state of the ESS; it is zero when the storage state x_k^s is higher than the reference value $\bar{C}_{s,t}$, and it takes positive otherwise. The generation cost $c_{g_f,k}^{f}$ represents the economic value of fossil fueled generation, with the same conversion efficiency used in the first layer. The cost coefficients in matrixes Q, K, and the remaining coefficients $\hat{k}_{um}$, $\hat{k}_{cu}$, have been set based on a sensitivity analysis on the case study.

2.2.2. General constraints for each unit

The dynamic behavior of the microgrid units is represented by a linear discrete-time state-space model, whose matrixes are derived from the linearization of the original non-linear continuous state function in correspondence of the current initial operating point. The resulting constraints are represented in eq. (9), (10):

$$x_{sc,k+1}^{i} = \boldsymbol{A}^{i} x_{sc,k}^{i} + \boldsymbol{B}^{i} u_{sc,k}^{i};\quad \forall\ i,k,sc \tag{9}$$

$$y_{sc,k}^{i} = \boldsymbol{C}^{i} x_{sc,k}^{i} + \boldsymbol{D}^{i} u_{sc,k}^{i};\quad \forall\ i,k,sc \tag{10}$$

For each scenario, the sMPC determines the control variable $u_{sc,k}^{i}$ as the sum of two contribution: the reference signal from the upper level $\bar{U}_k^i$ (with k consistent with the related first-layer timestep t) and the scenario-specific real-time set-point correction $\delta u_{sc,k}^{i}$, which is a function of the uncertainty manifestation (*i.e.* forecast error) $\hat{\xi}_{sc,k}^{gd}$ according to the affine policy shown in eq. (12). Different responses are defined depending on the value of the forecast error, effectively splitting the uncertainty space into two regions and resulting in a piecewise affine policy with a breakpoint in $\hat{\xi}_{k\,TRSH}^{gd}$.

$$u_{sc,k}^{i} = \bar{U}_k^i + \delta u_{sc,k}^{i};\quad \forall\ i,k,sc \tag{11}$$

$$\delta u_{sc,k}^{i} = \sum_{gd} \left[\left(m_k^{i+} \cdot \hat{\xi}_{sc,k}^{gd+} + q_k^{i+} \right) + \left(m_k^{i-} \cdot \hat{\xi}_{sc,k}^{gd-} + q_k^{i-} \right) \right];\quad \forall\ i,k,sc \tag{12}$$

$$m_k^{i+} \cdot \hat{\xi}_{k\,TRSH}^{gd} + q_k^{i+} = m_k^{i-} \cdot \hat{\xi}_{k\,TRSH}^{gd} + q_k^{i-}\quad \forall\ i,k,sc \tag{13}$$

Where: $\hat{\xi}_{sc,k}^{gd\,+}$, $\hat{\xi}_{sc,k}^{gd\,-}$, are the values of the uncertainty in the piecewise formulation.

In particular:

$$\hat{\xi}^{gd+}_{sc,k} = \begin{cases} \hat{\xi}^{gd}_{sc,k} & \hat{\xi}^{gd}_{sc,k} \geq \hat{\xi}^{gd}_{k\ TRSH} \\ 0 & \text{otherwise.} \end{cases}; \quad \forall\ k, sc \tag{14}$$

$$\hat{\xi}^{gd-}_{sc,k} = \begin{cases} \hat{\xi}^{gd}_{sc,k} & \hat{\xi}^{gd}_{sc,k} < \hat{\xi}^{gd}_{k\ TRSH} \\ 0 & \text{otherwise.} \end{cases}; \quad \forall k, sc \tag{15}$$

The state-state space formulation is a general way to represent the dynamic behavior of the units, but further constraints are required to fully characterize the various subsystems of the microgrid. The following sections introduce the set of technical constraints that model the dispatchable generators and storage systems, in addition to the state-space equations.

2.2.3. Programmable generators constraints

The following constraints represent the operating space of the generators, in terms of minimum and maximum power output when the generator is on, ramp-up and ramp-down limitations, and fuel consumption according to the generators' part-load curve.

$$\hat{U}^{g}_{min}\bar{Z}^{g}_{k} \leq u^{g}_{sc,k} \leq \hat{U}^{g}_{max}\bar{Z}^{g}_{k}; \quad \forall\ g, k, sc \tag{16}$$

$$u^{g}_{sc,k} - u^{g}_{sc,k-1} < \widehat{\Delta U}^{g}_{UP}\Delta t' + \overline{SU}^{g}_{k} \cdot \hat{U}^{g}_{max,SU}; \quad \forall\ g, k, sc \tag{17}$$

$$u^{g}_{sc,k} - u^{g}_{sc,k-1} > \widehat{\Delta U}^{g}_{DW}\Delta t' + \overline{SD}^{g}_{k} \cdot \hat{U}^{g}_{max,SD}; \quad \forall\ g, k, sc \tag{18}$$

$$f^{g_f}_{sc,k} = \hat{m}^{g_f}_{f}\, y^{g}_{sc,k} + \hat{q}^{g_f}_{f}\bar{Z}^{g}_{k}; \quad \forall g_f, k, sc \tag{19}$$

Where, $\bar{Z}^{g}_{k}$ represents the commitment status of the generator, identified by the first layer, $\overline{SU}^{g}_{k}$ and $\overline{SD}^{g}_{k}$ represents the start-up and shut-down flags, $\hat{U}^{g}_{min}$ and $\hat{U}^{g}_{max}$ are respectively the minimum and maximum value of the output of the generator when it is committed, $\widehat{\Delta U}^{g}_{UP}$ and $\widehat{\Delta U}^{g}_{DW}$ impose the limitation on ramping the units, $\hat{U}^{g}_{max,SU}$ and $\hat{U}^{g}_{max,SD}$ are the maximum variations during start-up and shut-down phases. The fuel consumption $f^{g_f}_{sc,k}$ is linearized according to Eq. (19) with respect to the generators' output $y^{g}_{sc,k}$. There could be generators that receive as input forms of energy produced internally, as opposed to external fuels (*e.g.,* electric-powered machinery); in this case, the relationship between input good and output good is implied in their state-space model.

2.2.4. Storage systems constraints

The description of the ESS is not univocal, as different storage systems can have limitation on their management, when dealing with their charge/discharge behavior. On the other hand, simple ESS, such as the storage tank for desalinated water, have no limitation on the simultaneity of charge and discharge, with unitary efficiency of those processes [45]. Two different sets of constraints are proposed to model the ESS, corresponding to two levels of physical soundness. Eqs. (20), (21) represents the general constraints on minimum/maximum storage capacity and maximum charge/discharge, which are always considered. If the ESS allows concurrent charge and discharge with unitary efficiency, the formulation relies on eq. (22), (23).

General storage constraints

$$\hat{C}^{s}_{min} \leq C^{s}_{sc,k} \leq \hat{C}^{s}_{max}; \quad \forall s, k, sc; \tag{20}$$

$$0 \leq u^{s,dh}_{sc,k} \leq \hat{U}^{s}_{max}; \hat{U}^{s}_{min} \leq u^{s,ch}_{sc,k} \leq 0; \quad \forall s, k, sc \tag{21}$$

Storage constraints for simultaneous charge and discharge mode

$$u^{s}_{sc,k} = u^{s,dh}_{sc,k} + u^{s,ch}_{sc,k}; \quad \forall\ s \notin s^{NS}, k, sc \tag{22}$$

$$C^{s}_{sc,k+1} = C^{s}_{sc,k} - \left(u^{s,ch}_{sc,k} + u^{s,dh}_{sc,k}\right)\Delta t' - \hat{L}^{s}\Delta t'; \quad \forall s \notin s^{NS}, k, sc \tag{23}$$

Where: $\hat{C}^{s}_{min}$ and $\hat{C}^{s}_{max}$ are the boundaries for the storage content, $\hat{U}^{s}_{min}$ and $\hat{U}^{s}_{max}$ limits the input and output fluxes, $u^{s}_{sc,k}$ represents the net flux at the storage bus, sum of the discharge and charge components $u^{s,dh}_{sc,k}, u^{s,ch}_{sc,k}$. In this formulation, $u^{s,dh}_{sc,k} \geq 0$ and $u^{s,ch}_{sc,k} \leq 0$, as they are referred to the balance on the bus of the microgrid.

The formulation for the BESS must rely on different constraints, employing the auxiliary variable z^{s}_{k} to enforce the non-simultaneity of input and output power. In this way when $z^{s}_{k} = 1$, only charge is allowed, and vice versa if $z^{s}_{k} = 0$ (see the eq (24), (25) below):

$$0 \leq u^{s,dh}_{k} \leq \left(1 - z^{s}_{k}\right)\hat{U}^{s}_{max}; \quad \forall\ s \notin s^{NS}, k \tag{24}$$

$$z^{s}_{k}\hat{U}^{s}_{min} \leq u^{s,ch}_{sc,k} \leq 0; \quad \forall\ s \notin s^{NS}, k, sc \tag{25}$$

The latter constraints cannot be directly implemented in the sMPC formulation, as the affine response of the BESS is evaluated for the power at the AC bus, controlled by $u^{s}_{sc,k}$. To act on this variable while linking all the scenarios of the optimization problem, the following constraints are considered Eqs. (26)-((32)). The introduction of the auxiliary variables $z^{s}_{sc,k}$, $Aux^{s}_{sc,k}$ is needed to address the scenario-dependent solution, while $\hat{U}^{s}_{Aux}$ is a parameter acting as Big-M for the constraints (28)(29). Moreover, $\hat{\sigma}^{s}_{k}$ is a parameter indicating when the storage system has reached the maximum charge, forcing the RES generation systems to work in reduction power point tracking (RPPT); the introduction of this parameter has been proven helpful, speeding up the solution time during RPPT.

Storage constraints for non-simultaneous charge and discharge mode

$$u^{s,ch}_{sc,k} = u^{s}_{sc,k} \cdot \eta^{s}_{ch}; \quad u^{s,dh}_{sc,k} = u^{s}_{sc,k}/\eta^{s}_{dh}; \quad \forall\ s \in s^{NS}, k, sc \tag{26}$$

$$z^{s}_{sc,k}\hat{U}^{s}_{min} - \hat{L}^{s}\hat{\sigma}^{s}_{k} \leq u^{s}_{sc,k} \leq \hat{U}^{s}_{max}\left(1 - z^{s}_{sc,k}\right); \quad \forall s \in s^{NS}, k, sc \tag{27}$$

$$u^{s,ch}_{sc,k} - \left(1 - z^{s}_{sc,k}\right)\hat{U}^{s}_{Aux} \leq Aux^{s}_{sc,k} \leq u^{s,ch}_{sc,k} + \left(1 - z^{s}_{sc,k}\right)\hat{U}^{s}_{Aux}; \quad \forall s \in s^{NS}, k, sc \tag{28}$$

$$u^{s,dh}_{sc,k} - z^{s}_{sc,k}\hat{U}^{s}_{Aux} \leq Aux^{s}_{sc,k} \leq u^{s,dh}_{sc,k} + z^{s}_{sc,k}\hat{U}^{s}_{Aux}; \quad \forall s \in s^{NS}, k, sc \tag{29}$$

$$C^{s}_{sc,k+1} = C^{s}_{sc,k} - Aux^{s}_{sc,k}\Delta t' - L^{s}\Delta t'; \quad \forall s \in s^{NS}, k, sc \tag{30}$$

$$z^{s}_{sc,k} \leq 1 - \hat{\sigma}^{s}_{k} \quad \forall s \in s^{NS}, k, sc \tag{31}$$

$$z^{s}_{sc,k} \in \{0, 1\}, Aux^{s}_{sc,k} \in \mathbb{R} \quad \forall S \in s^{NS}, k, sc \tag{32}$$

Where:

$$\hat{\sigma}^{s}_{k} = \begin{cases} 1 & \text{if } \tilde{C}^{s}_{sc,0} \geq \hat{C}^{s}_{max} - \varepsilon \\ 0 & \text{otherwise} \end{cases}. \tag{33}$$

$$x^{s}_{sc,k} = C^{s}_{sc,k}; \ y^{i}_{sc,k} = u^{s}_{sc,k} \tag{34}$$

The latter constraints (26)-(34) describe the correct behavior of the BESS systems. Indeed, for the scenarios that require BESS discharge $z^{s}_{sc,k} = 0$, then $0 \leq u^{s}_{sc,k} \leq \hat{U}^{s}_{max}$ and $Aux^{s}_{sc,k} = u^{s,dh}_{sc,k}$, from constraint (29); in this case, the constraint (28) is not limiting, as it becomes $-\hat{U}^{s}_{Aux} \leq Aux^{s}_{sc,k} \leq \hat{U}^{s}_{Aux}$. During BESS charge, $z^{s}_{sc,k} = 1$, thus, $\hat{U}^{s}_{min} \leq u^{s}_{sc,k} \leq 0$ and $Aux^{s}_{sc,k} = u^{s,ch}_{sc,k}$. Furthermore, if RPPT is required, $\hat{\sigma}^{s}_{k} = 1$, only discharge will be allowed (see constraint (32)), and the charging power is no longer limited by $\hat{U}^{s}_{min}$ but by $\hat{L}^{s}$. For BESS coupled with inverters, the parameter $\hat{L}^{s}$ represents the consumption of the auxiliary systems of the inverter, which withdraw power directly from the BESS. The parameters representing the storage efficiency (η^{s}_{ch}, η^{s}_{dh}) are constant values that include both BESS and inverter/rectifier efficiencies. The combination of $\hat{L}^{s}$, η^{s}_{ch}, η^{s}_{dh} leads to a characterization of a variable efficiency of

the whole BESS and inverter system, even though those parameters are constant.

The indications in (34), identifies the matching between the state-space representation and the storage constraints formulation; while the storage internal state is represented by its energy content C^s, the distinction between set-point and power output is neglected. This is true for BESS, as the coupled inverter works at a much higher bandwidth than the second-layer control. Regarding other types of storage systems characterized by a slower response to power set-points or strongly non-linear characteristics (*e.g.,* thermal storage), the previous constraints are no longer valid, and a different formulation would be required, which is out of the scope of this work.

2.2.5. Good balance constraint

The following constraints ensure that the demand of each good $\hat{D}^{gd}_{sc,k}$ is satisfied for each scenario, combining the output of all the units of the MG. In this formulation, the possibility of unmet demand and curtailment are implicitly represented in the state space representation, indeed both are considered as virtual units with instantaneous response, meaning that $y^{um}_{sc,k} = u^{um}_{sc,k}$ and $y^{cu}_{sc,k} = u^{cu}_{sc,k}$.

$$\sum_i y^i_{sc,k} \cdot \hat{\chi}^{i,gd} = \hat{D}^{gd}_{sc,k}; \quad \forall i,k,sc \tag{35}$$

Where:

$$\hat{\chi}^{i,gd} = \begin{cases} 1 & \text{If unit is producing good } gd; \\ -1 & \text{If unit is consuming good } gd; \\ 0 & \text{If unit } i \text{ is not participating in the production/} \\ & \text{consumption of good } gd \end{cases} \quad \forall i, gd, k, sc \tag{36}$$

If unit i is not participating in the production/consumption of good gd.

$$\hat{D}^{gd}_{sc,k} = \bar{D}^{gd}_k - \hat{\xi}^{gd}_{sc,k} \quad \forall gd, k, sc \tag{37}$$

The parameter $\hat{D}^{gd}_{sc,k}$ represents the net demand of good gd for scenario sc at time step k. For instance, when the good is electric power, $\hat{D}^{gd}_{sc,k}$ is the difference between the electric load and the total renewable generation (before the eventual curtailment if required). The parameter $\hat{\chi}^{i,gd}$ is the participation factor of unit i for the good balance; in particular, for unmet demand and curtailment, the parameters are set as $\hat{\chi}^{um,gd} = 1$ and $\hat{\chi}^{cu,gd} = -1$.

2.3. Second-layer model of EMS_{PI}

The developed second layer based on sMPC is compared against a real-time non-predictive method which makes use of the predicted solution to continuously balance the MG production (EMS_{PI}). It is based on proportional-integral (PI) control, in charge of SOC tracking of the BESS systems. From the on-field measurements of actual SOC, the PI computes the total required variation of power output from programmable generation, complying with their ramp limitations, to follow as close as possible the SOC trajectory evaluated by the first layer. Then, a linear program is solved to optimize the power sharing among those units. The detailed description of the algorithm can be found in [21].

3. Online EMS implementation and experimental set-up

The optimization problems described in section 2 are the core of the hierarchical EMS proposed in this paper. In this work, the first layer problem is defined over a horizon of 24 hours, with a resolution of 15 minutes; forecasts profiles for demand and RES production are generated accordingly. On the other hand, the second layer works with a resolution of 1 minute, with forecast horizon up to 15 minutes if sMPC is employed. The forecasting module is employed to provide the expected values of critical electricity demand (corresponding to the non-programmable electric loads) and water demand, as well as wind and PV generation (if present in the MG configuration under study). A seasonal autoregressive integrated moving average (SARIMA) model is used for the medium-term prediction of electrical loads, water demand, and wind power, as in [25], based on historical time series of the related profiles [46].On the contrary, ARIMA model are outperformed by artificial intelligence algorithms in predicting PV production [47], therefore PV generation forecasts are obtained through neural networks, trained on the historical data collected at the MG^2Lab [48] These profiles will constitute the input for the first-layer optimization model. Additionally, the sMPC requires as inputs the scenarios of forecast errors of the net demand profiles for all goods (*i.e.,* good demand minus the related renewable generation). The scenarios are obtained through Monte Carlo simulation of expected forecast errors by an ARIMA model, whose parameters have been estimated based on past measurements of forecast errors ($\xi^{gd}_{t'}$ for $t' = 0 \dots k$) through least-squared fitting of the model. The PV forecast considered in the second layer is based on a persistent model along the sMPC optimization horizon, therefore the PV forecast error is the difference between the predicted value and the last PV output measurement. This error is then combined with the Monte Carlo simulation of the ARIMA model to obtain the error of net electricity demand. The net demands scenarios are then determined subtracting the simulated forecast errors to the value of the net demand considered in the first layer (see eq. (37)). There are two contrasting needs regarding the selection of representative scenarios. A large number of scenarios would be required, to have a good representation of all the possible outcomes of the uncertainty, while a small set of scenarios is desirable to reduce the computational complexity and solving time of the sMPC. For this reason, several scenarios (≥ 500) are obtained through Monte Carlo simulation, as in [31]; then, a scenario reduction technique is implemented, following the algorithms in [49].

Both the EMS_{PI} and EMS_{sMPC} are tested and validated experimentally. The online implementation was done using Matlab, directly communicating with the PLC of the microgrid; its architecture is shown in Figure 4 and a schematic representation of the information flow in the EMS, together with the indication of the task periods in given in Figure 5.

The MILP problems are formulated through YALMIP [50] and solved with Gurobi [51] on a on a workstation with Intel® Core™ i9-7900X CPU @ 3.3 GHz. The two-layer structure is arranged on two separate workspaces and the cyclic tasks are performed through timer objects, built-in Matlab functions to schedule periodic commands:

- The first workspace corresponds to the first-layer of the hierarchical EMS, thus, it includes the forecasting module and the optimization module. The first-layer MILP is solved considering as termination criteria a MIP gap of 1% and a maximum time limit of 1 minute.
- The second workspace manages the communication with the PLC, through the MODBUS interface, with a period of 20 seconds. When employing EMS_{sMPC}, the optimization of the second-layer problem is performed in this workspace, within a cyclic task with a period of 1 minute; then, the control decisions and the correction rules are sent to the PLC. The stochastic solution is obtained for a MIP gap of 1% and a maximum solution time of 30 seconds. On the other hand, the second layer of the EMS_{PI} is directly implemented in the PLC. In this case, the communication module only sends the tentative ED and the reference SOC trajectory to be tracked during the advancement period. The PLC performs its tasks with a resolution of 100 ms, as common industrial practice.

The workspaces communicate through the exchange modules, executed every 20 seconds: while one exchange module sends the required measurements to the first-layer block, the other one sends the scheduling solution to the second layer. The periods of the cyclic tasks are chosen according to the viability of the implementation in the experimental set-up. In particular, the communication time between Matlab and PLC was set to 20 seconds as a compromise between fast communication (*i.e.,* frequent monitoring of the microgrid status) and idle time requirements of the Matlab software among consecutive tasks, imposed by the exchange

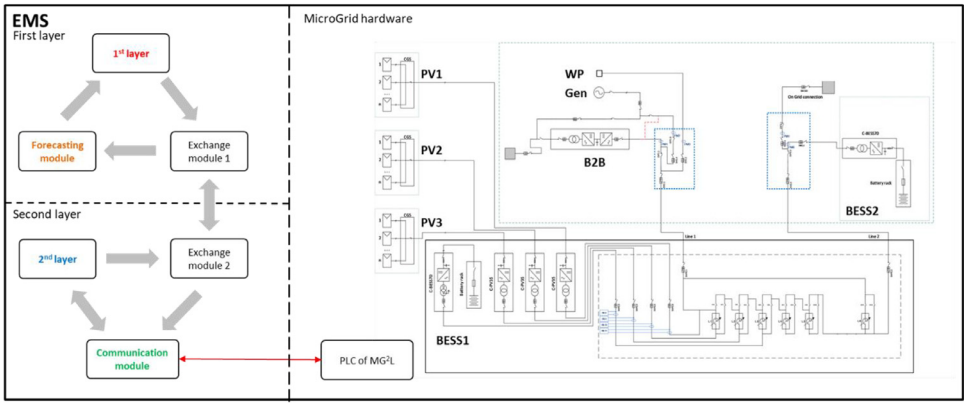

Fig. 4. Online EMS architecture and experimental set-up.

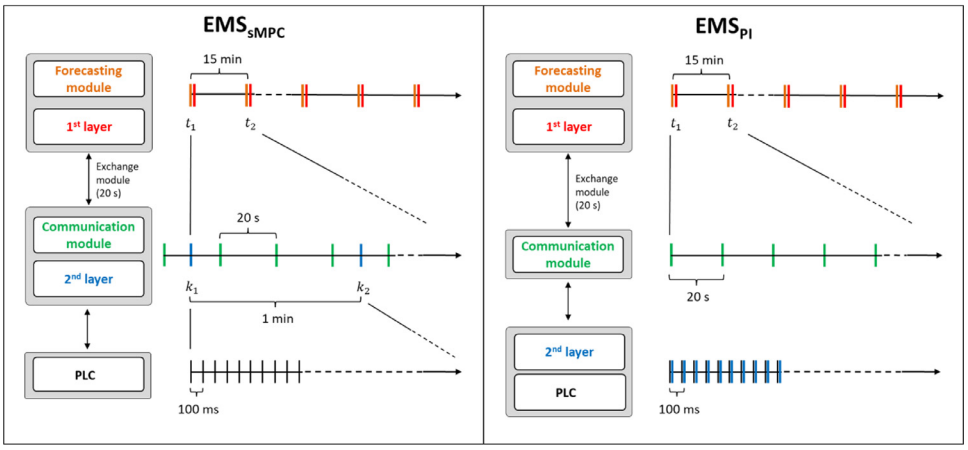

Fig. 5. EMS structure and tasks period.

module and the sMPC solution time. The average solution time is about 20 seconds for the first-layer model, and about 5 seconds for the second layer.

4. Model validation

This section introduces the case study employed for the validation of the proposed EMS. The experimental activities were carried out at MG^{2}Lab, a low-voltage multigood microgrid at the Department of Energy of Politecnico di Milano whose complete description can be found [22, 41].

4.1. Case study definition

The case study is defined so to assess the level of accuracy of the simulation compared to the actual behavior, to validate the proposed numerical models and certify the relevance of the numerical results.

The configuration considered for this study aims at emulating the operation of a rural MG, providing electricity and potable water to its users. Specifically, the set-up comprises:

- Three PV fields, for a total installed capacity of 75 kW$_p$.
- A Back-To-Back (B2B) converter, simulating a net electric load profile (in this study, the profile consists of electric load minus wind generation).
- Two identical 70 kW/67.5 kWh battery energy storage systems, from now on named as BESS$_1$ and BESS$_2$.
- A 25 kW$_{el}$ asynchronous generator, fueled by natural gas (ICE).
- A reverse osmosis desalination system, or water purifier (WP), with an associated water tank, to increase the flexibility of potable water production.

Table 1
Technical limits of controllable units.

	Min out	Max out	Ramp limit
BESS1/2	-70 kW	+70 kW	—-
ICE	12.5 kW	25 kW	3 kW/min
WP	650 L/h	1000 L/h	150 L/min

The technical limitations of the controllable assets are summarized in Table 1. The MG^{2}Lab has been operated in islanded mode, with one BESS inverter operating in stiff grid-forming mode, and the other one in grid following mode. Thus, the former imposes frequency and voltage to the microgrid system and acts as slack-node for both active and reactive power, while the latter precisely follows the active power setpoints calculated by the EMS. As a matter of fact, the reactive power flow has not been considered in the EMS control layers since the limited extension of the experimental facility coupled with the low voltage of the system (*i.e.,* 400 V) and the low load level of the lines made the system equivalent to a single node system. The whole voltage regulation has thus been assigned to the grid-forming inverter. The programmable generator has been simulated with a first-order transfer function and the resulting output power has been subtracted from the net profile of the B2B to provide the right energy balance in the islanded microgrid.

All the power measures have been acquired through the PLC network thanks to the dedicated power measurement modules properly connected to line voltages and class-1 current transformers. As far as the BESS SOC is concerned, the integrated Battery Management Systems (BMS) directly provided these measurements and made them available through MODBUS communication to the PLC. The BMS estimates the SOC using a combined approach that exploits both current and voltage methods. The former measures the SOC through continuous current in-

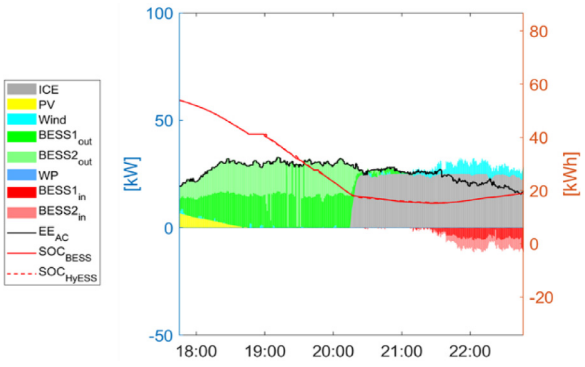

Fig. 6. Power and BMS measurements example.

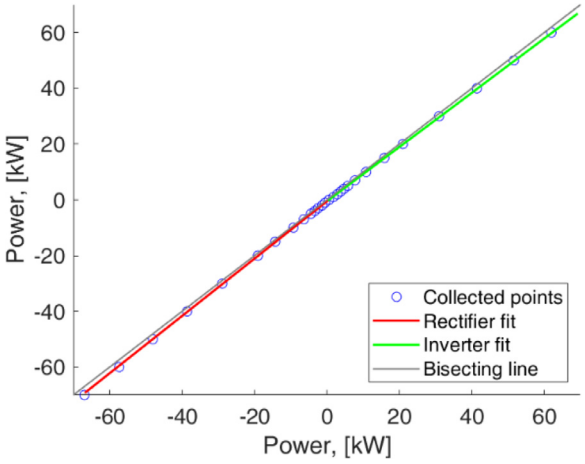

Fig. 8. BESS inverter-rectifier input-output characteristic.

tegration over time, while the latter corrects the drifting of the current method by updating the SOC through look-up-tables and voltage measurements when certain SOC levels are reached (*i.e.,* 60%, 40% and 8%). As it is possible to notice in Figure 6, around 19:00, during the discharge phase of the batteries, the BMS stops updating the SOC value, while it continues discharging, until the previous indication matches the correct value.

Electric load and wind generation profiles are taken from the data provided by Engie-EPS [52], and scaled to values compatible with MG^{2}Lab assets, while the water demand has been estimated by the NREL tool [53]. Typical profiles employed in MG^{2}Lab operations are reported in Figure 7. In the next sections, the normalized root mean squared error (nRMSE) is used as error metric to quantify forecast accuracy; the normalization is given dividing the RMSE by the maximum observed value during the considered interval.

During the experimental operation, when employing the EMS$_{\text{sMPC}}$, the set-point correction rules are updated every minute at software level, and then sent to the PLC, that stores them until a new solution is received: the commands consist in the reference set-points $\bar{U}_{i,t}$ and the coefficients m_k^{i+}, q_k^{i+}, m_k^{i-}, q_k^{i-}. However, the set-point correction is applied according to the PLC resolution, following eq. (12), as the PLC constantly measures the actual forecast error: a continuous adaptation of the power sharing among the units is then achieved. The numerical simulations need to mimic PLC tasks assignment and feedback to the EMS. This is done adding an external layer, called *MG status estimation*, which evaluates the states of the units according to their transfer function with PLC time discretization. In this way it is possible to account for all the communication delays elapsed during the experimental activities between the MG and the EMS, reducing the mismatch between numerical simulation and the experiments. Indeed, there is always a lag of 10 second between the collection of the measurements by the communication layers and the initialization of sMPC, while a longer lag (up to 2 minutes) is found between the reading of the inputs for the first-layer optimization and the collection of the solution by the second layer. The EMS$_{\text{PI}}$ has a simpler structure: the second-layer control is directly implemented in the PLC, therefore, there is no need to differentiate the time discretization between the control decisions and their actuation. In the *MG status estimation*, the efficiency of BESS and inverter is no longer kept constant. The variable efficiency of the coupled BESS/inverter unit is considered according to a measurement campaign (Figure 8).

Numerical simulations are carried out after the experiment, to collect the relevant measurements required to run the simulations (such as the actual load profile of the B2B and PV production). Regarding the real PV production, when the fields are operated in RPPT, the required PV curtailment is estimated by determining the PV output at MPPT, through irradiation and temperature measurements and adopting the power coefficient approach [54].

4.2. Experimental EMS$_{\text{sMPC}}$

This section shows the results of two days of MG^{2}Lab operation with EMS$_{\text{sMPC}}$ and the comparison with the respective numerical simulations.

Table 2 details the summary of energy fluxes during two days of operation, while Figure 9 shows the experimental and simulated profiles. The simulated MG operating profiles comply with the observed experimental operation, in terms of commitment and operating cost; the simulated fuel consumption is very close to the measured value, main component of the EMS objective function. It is important to point out that

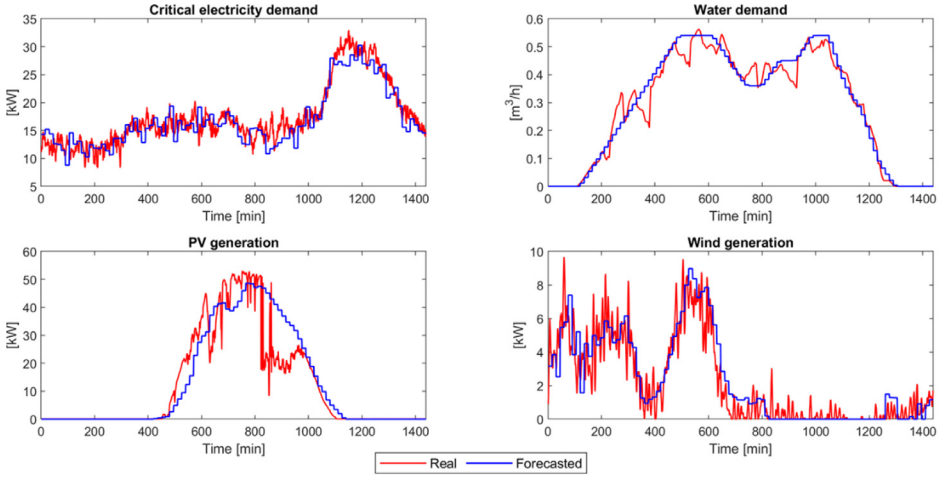

Fig. 7. Example of demand and generation profiles for one day of MG operation.

Table 2
Energy summary of experimental MG²Lab operation and comparison with numerical simulation for EMS_{sMPC}.

EMS_{sMPC}			Day 1		Day 2	
			Experimental	Simulated	Experimental	Simulated
nRMSE	**Critical electricity demand**	[%]	6.01		6.71	
	Water demand	[%]	18.15		12.08	
	PV generation	[%]	10.21		13.42	
	Wind generation	[%]	5.89		6.92	
Critial electricity demand		[kWh]	413.8		417.0	
Total electricity demand		[kWh]	452.7	453.0	459.1	462.1
ICE generation		[kWh]	183.6	185.0	192.7	197.3
PV generation		[kWh]	267.2	267.8	287.7	284.2
Wind generation		[kWh]	69.9	69.4	53.3	52.4
RES curtailment[1]		[kWh]	8.2	8.1	34.0	38.4
Unmet electricity demand		[kWh]	0.0	0.0	0.0	0.0
Battery discharge		[kWh]	126.3	120.4	127.3	119.5
Battery charge		[kWh]	192.3	189.7	195.1	191.4
Final Storage Energy		[%]	17.8	17.4	18.0	21.2
Fuel Consumption		[Nm^3]	63.2	63.4	65.3	66.9
Δ fuel consumption		[%]	—-	0.15	—-	2.38

[1] RES curtailment value is not reliable, as it is computed from an estimate of PV generation

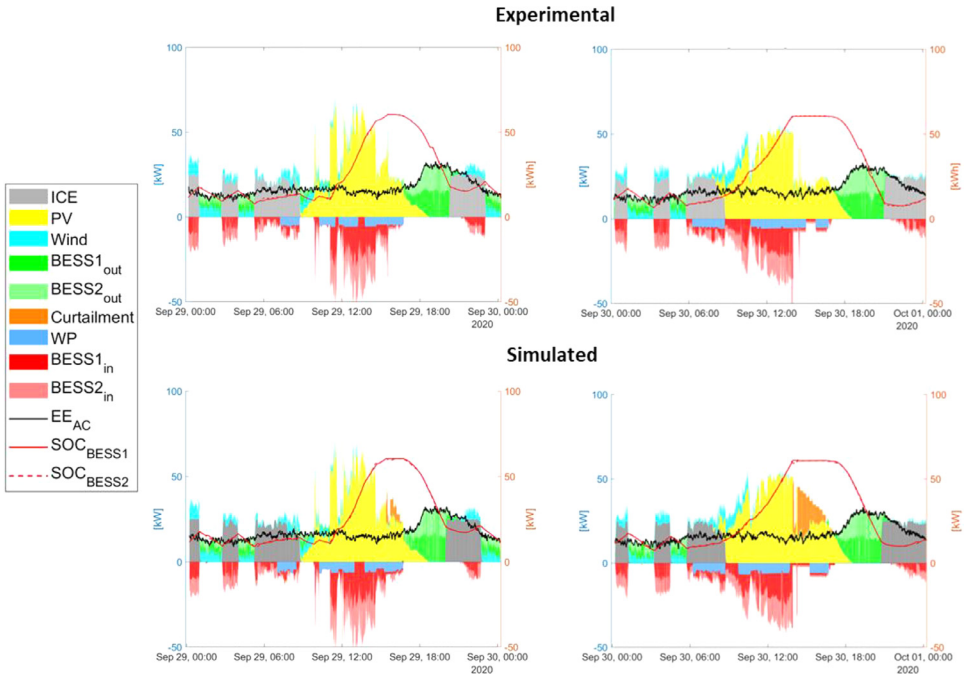

Fig. 9. Experimental and simulated profiles with EMS_{sMPC}. The plots on the left refer to day 1, the ones on the right refer to day 2.

even limited variations between the measured values of the MG status and the ones obtained by *MG status estimator* can affect the solution of the MILP problems. The differences of the operations can be attributed to a slightly different management of the water purifier. Moreover, a crucial role is played by SOC estimation, whose value affects both the scheduling and the tracking problem. Indeed, there is a discrepancy between the measurements and the simulated energy fluxes through the BESS, that cannot be corrected in the numerical simulation, due to the working principle of the BMS. During day 1, simulation and experiment show similar final storage energy content. Looking at the experiment, the BMS updates, occurring at SOC 40% and 20% during the evening discharging phase, did not refresh the SOC measures while cumulatively 7.4 kWh were discharged by both BESS, amount compatible with the total difference between the estimated and the measured energy fluxes (of about 6.5 kWh). The numerical simulation, where no BMS update is considered, anticipates by 15 minutes the start-up of the ICE generator, but keeps the same number operating hours. In day 2, a slightly different behavior is observed. Even though the BMS missed 8.3 kWh, value coherent with the difference in energy discharged between experiment and simulation (7.8 kWh), the EMS decisions in the simulation led to a higher production from the ICE generator anticipating its start-up of 15 minutes, thus, increasing the number of operating hours, resulting also in a higher final SOC. Figure 10 underlines the ICE management, both in terms of commitment and control actions. At the beginning of the day, when the estimated SOC is in agreement to the measured one, the simulated sMPC behaves very closely to what observed experimentally, whereas, during the operation, the cumulated SOC estimation error affects the control decision, leading to a slightly different dispatch (Figure 11).

4.3. *Experimental EMS_{PI}*

The validation of the EMS also includes the architecture with PI control as second layer, analyzing two days of operation. The comparative results are reported in Table 3.

During the first day, due to cloudy conditions, low PV yield was observed, that affected the charging phase of the BESS, as the maximum

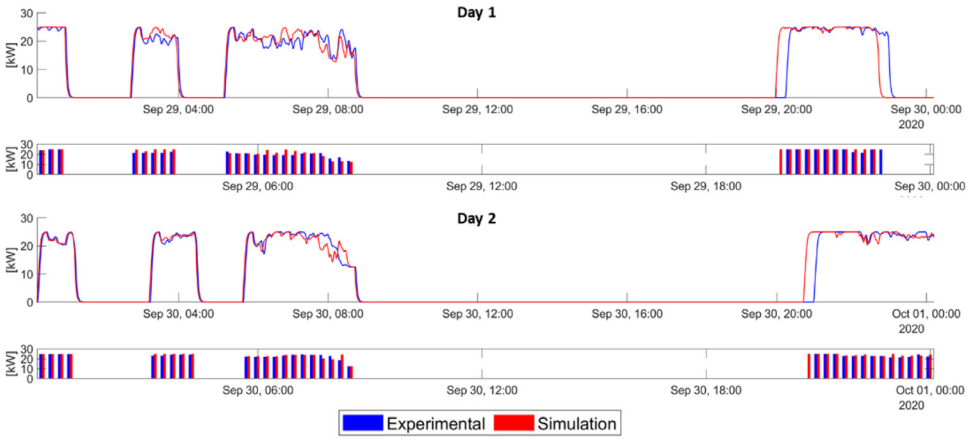

Fig. 10. ICE commitment and power output comparison between experiment and simulation with EMS_{sMPC} for day 1 (top figure) and day 2 (bottom figure).

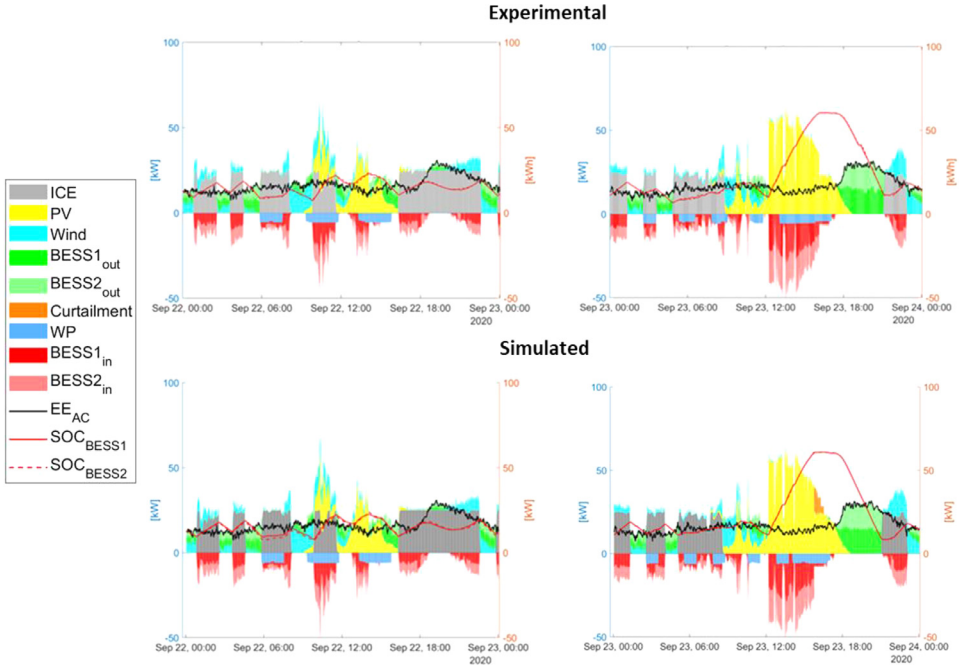

Fig. 11. Experimental and simulated profiles with EMS_{PI}. The plots on the left refer to day 1, the ones on the right refer to day2.

Table 3
Energy summary of experimental MG²Lab operation and comparison with numerical simulation for EMS_{PI}.

EMS_{PI}			Day 1		Day 2	
			Experimental	Simulated	Experimental	Simulated
nRMSE	**Critical electricity demand**	[%]	6.75		8.14	
	Water demand	[%]	24.01		26.22	
	PV generation	[%]	9.30		8.72	
	Wind generation	[%]	5.05		7.49	
Critial electricity demand		[kWh]	413.8		393.8	
Total electricity demand		[kWh]	431.6	433.0	451.6	452.1
ICE generation		[kWh]	305.5	309.0	183.2	191.3
PV generation		[kWh]	93.2	92.7	259.8	256.1
Wind generation		[kWh]	94.5	94.2	82.3	82.0
RES curtailment		[kWh]	0.0	0.0	2.7	6.7
Unmet electricity demand		[kWh]	0.0	0.0	0.0	0.0
Battery discharge		[kWh]	84.5	81.9	136.2	127.5
Battery charge		[kWh]	145.1	144.7	206.9	204.8
Final Storage Energy		[%]	16.4	16.7	20.6	20.7
Fuel Consumption		[Nm^3]	103.2	104.0	62.5	64.7
Δ fuel consumption		[%]	—-	0.76	—-	3.40

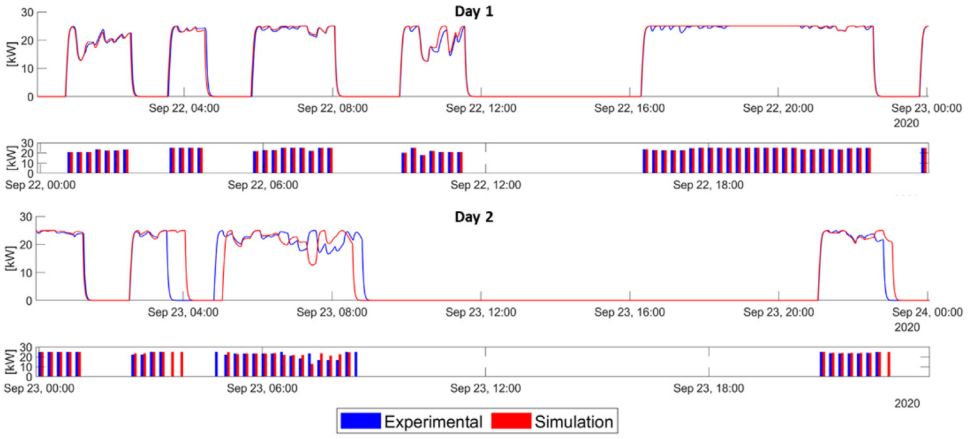

Fig. 12. ICE commitment and power output comparison between experiment and simulation with EMS_{PI} for day 1 (top figure) and day 2 (bottom figure).

Table 4
Test case characteristics.

	Peak	Daily demand or generation	nRMSEEMS [%]	nRMSEPF-EMS [%]	nRMSEPF-MILP [%]
Critical electricity demand	65 kW	831.7 kWh	6.12	3.93	0.00
Water demand	1 m^3/h	10.0 m^3	6.08	3.54	0.00
PV generation	75 kW	488.8 kWh	7.98	6.03	0.00
Wind generation	40 kW	201.8 kWh	29.19	11.97	0.00

SOC reached during the day was about 35 %. For this reason, no BMS update occurred during the experiment, and a limited mismatch between simulated and experimental quantities related to the BESS is observed (in terms of energy fluxes and final SOC). The remaining differences can be addressed to uncertainty of measurements and fitting errors of the non-linear efficiency of the BESS/inverter units, used in *MG status estimation*. The absence of high discrepancy in between measured and estimated SOC leads to a very high compatibility of simulated operation with experimental ones. Indeed, the same schedule of ICE generator and very similar dispatch can be noticed, as shown in Figure 12.

On the other hand, on day 2, a larger mismatch between experimental results and numerical simulations was observed. Considering the first part of the day, the first layer in the numerical simulation computes a different commitment of the ICE, which starts to diverge at 3:30, even though, in both the experiment and the simulation, the ICE followed the same dispatch, and the was no relevant difference in SOC up to that moment. On the other hand, the number of ICE operating hours until 9:00 remains unaffected. Considering the remaining part of the day, the BMS update occurring during the discharge phase miscounted 11.3 kWh of energy provided by the BESS, amount that the simulated EMS decided to supply employing the ICE for one timestep more, leading to a higher fuel consumption.

5. Model application to a test case

This section introduces a comparative analysis based on numerical simulations of EMS_{PI} and EMS_{sMPC}. The EMS has been tested for an off-grid MG aimed at satisfying the demand of electricity and potable water of a small rural community, for two weeks of operation. Relevant data regarding the test case MG are taken from [52, 53], and summarized in Table 4 and Table 5.

The results of the optimal grid management based on EMS_{PI} and EMS_{sMPC} are reported in Table 6. The application of EMS_{sMPC}, instead of EMS_{PI},leads to a reduction of 2.7 % in fuel consumption, that is considered one of the key performance indexes when evaluating the effectiveness of the EMS. The fuel consumption is evaluated as the sum of fixed and variable fuel consumption, according to eq (19): the former represents the amount of fuel related to the commitment status of the generators, operated at minimum load; the latter is related to their actual power output.

Table 5
Characteristics of controllable units and technical limitations.

Generators			
	Min out	**Max out**	**Ramp limit**
G1	2.5 kW	10 kW	3 kW/min
G2	7.5 kW	20 kW	2 kW/min
G3	12.5 kW	25 kW	1.5 kW/min
WP	950 m^3/h	1500 m^3/h	150 m^3/min
Storages			
	Size	**SOC_{min}**	**SOC_{max}**
BESS	150 kWh	10%	90%
Water tank	5 m^3	0%	100%

Table 6
Results summary for the proposed EMS on the test case.

		EMS_{PI}	EMS_{sMPC}
Critial electricity demand	[kWh]	11643.5	
Total electricity demand	[kWh]	12687.0	12683.5
ICE generation	[kWh]	4800.5	4660.2
PV generation	[kWh]	5652.1	5903.1
Wind generation	[kWh]	2825.4	2720.3
RES curtailment	[kWh]	1191.1	1045.1
Unmet electricity demand	[kWh]	6.2	3.2
Final Storage Energy	[%]	37.6	30.3
$RMSE_{track}$	[kWh]	14.2	12.7
SOC surplus	[kWh]	1986.0	1448.8
SOC deficit	[kWh]	-1012.5	-1094.4
Fixed fuel consumption	[Nm^3]	805.9	828.3
Variable fuel consumption	[Nm^3]	782.4	716.0
Total fuel consumption	[Nm^3]	1588.3	1544.3
Δ fuel consumptions	[%]	—-	-2.7

The resulting operation cost can be traced back to the ability of the second layer to follow the reference SOC trajectory, preserving the energy fluxes optimized by the first layer; a SOC tracking error is observed, with a lower $RMSE_{track}$ when employing the sMPC. Generally speaking, a SOC overprediction is observed when the net demand is higher than forecasted, either because of insufficient total generation capacity or due to the impossibility of increasing the power output of the genera-

tors quickly enough to compensate for the unbalancing. It is important to notice that a SOC overprediction leads to an over-commitment by the next first layer update so to restore the spinning reserve. Conversely, a SOC underprediction represents an excessive generation due to the inability of reducing the power output of the programmable generators, because of ramp limits or minimum power output. In the simulations, EMS_{sMPC} causes a lower SOC surplus than EMS_{PI}, due to its capability of anticipating future forecast errors. Indeed, EMS_{sMPC} shows a responsive and efficient reduction of the power output of the committed generators when required, thus a lower variable fuel cost. On the other hand, the higher SOC surplus of EMS_{PI} leads to a saving in commitment cost with respect to EMS_{sMPC}, yet a larger variable cost: the generators operate closer to their maximum power output to guarantee the tracking, but the set-point reduction is not fast enough to reduce the SOC surplus once the negative deviation is balanced. All these aspects reflect in reduction of 12% of curtailment when employing EMS_{sMPC} instead of EMS_{PI}, favoring a larger RES penetration.

Once identified the advantages of sMPC with respect to the PI approach, it is important to understand the limits of EMS_{sMPC}. These limits are determined by introducing three benchmark approaches, which correspond to increasing level of solution accuracy, with the following differences in terms of inputs and second layer:

- $EMS_{PF\text{-}MPC}$ utilizes a deterministic optimization problem as second layer with a unique net demand profile, representing the actual future realization (perfect forecast). This benchmark is intended to give the best possible outcome by the application of an optimal second layer when forecast errors from the first layer are still present.
- PF-EMS has the same structure of $EMS_{PF\text{-}MPC}$, but the demand and generation profiles are given as the average of the real profiles corresponding to the related first-layer time step. In this way, the total amount of demand and RES generation seen by the first layer perfectly matches the actual ones, but there are still fluctuations to be balanced by the second layer. PF-EMS results will represent the best possible achievements, given exact forecasts with coarser time resolution than the one considered when dispatching the MG. Figure 13 shows the difference between the load demand profile used in all the EMS and in PF-EMS.
- PF-MILP corresponds to a single layer optimization problem, solved with the discretization of the EMS second-layer, thus, the real profiles of demand and RES generation are considered with the correct time resolution. In this case, reserve constraints are no longer enforced, as PF-MILP perfectly observes future profiles, making the re-

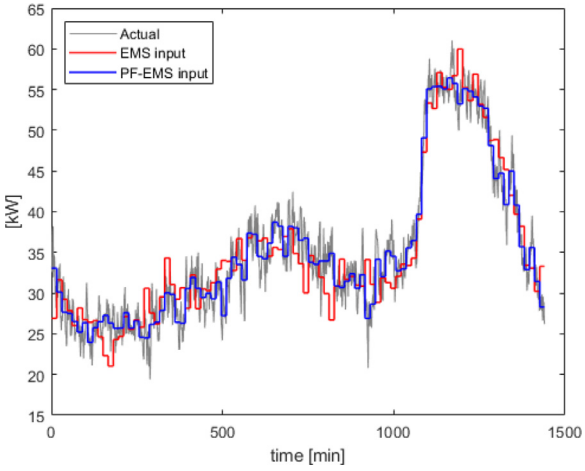

Fig. 13. Example of load demand profiles as input of the first layer of EMS and PF-EMS.

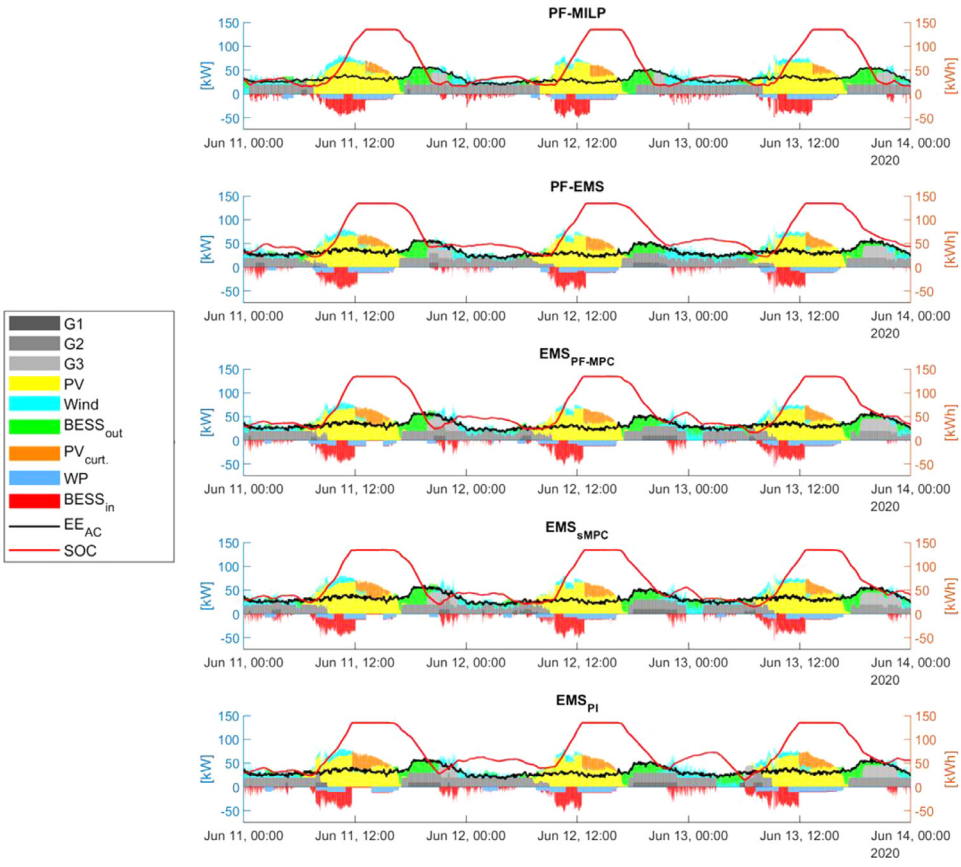

Fig. 14. Comparison of proposed EMS and benchmarks.

Table 7
EMS_{sMPC} and benchmarks results.

		EMS_{sMPC}	$EMS_{PF\text{-}MPC}$	PF-EMS	PF-MILP
Critial electricity demand	[kWh]	11643.5			
Total electricity demand	[kWh]	12683.5	12677.6	12689.5	12683.4
ICE generation	[kWh]	4660.2	4631.1	4474.0	4287.5
PV generation	[kWh]	5903.1	5918.1	5992.1	6591.4
Wind generation	[kWh]	2720.3	2728.8	2825.4	2796.2
RES curtailment	[kWh]	1045.1	1021.6	851.0	280.9
Unmet electricity demand	[kWh]	3.2	1.3	0.0	0
Final Storage Energy	[%]	30.3	28.8	35.1	12.5
$RMSE_{track}$	[kWh]	12.7	12.3	3.9	—-
SOC surplus	[kWh]	1448.8	1414.6	355.9	—-
SOC deficit	[kWh]	-1094.4	-974.8	-522.9	—-
Fixed fuel consumption	[Nm^3]	828.3	836.3	734.3	578.6
Variable fuel consumption	[Nm^3]	716.0	700.9	732.6	771.6
Total fuel consumption	[Nm^3]	1544.3	1537.2	1466.9	1350.2
Δ fuel cons. (wrt $EMS_{PF\text{-}MPC}$)	[%]	0.5	—-	—-	—-
Δ fuel cons. (wrt PF-EMS)	[%]	5.3	4.8	—-	—-
Δ fuel cons. (wrt PF-MILP)	[%]	14.4	13.9	8.6	—-

serve requirements unnecessary. This solution is the lower bound for the performance of all EMS.

A comparative analysis between the EMS_{sMPC} and the benchmarks is reported in Table 7, and sample profiles are shown in Figure 14. PF-EMS has a higher fuel consumption by 8.6% with respect to PF-MILP due to spinning reserve constraints, that are enforced in PF-EMS to ensure the MG capability of balancing forecast errors in the second layer. Moreover, inexact forecasts in the first layer of $EMS_{PF\text{-}MPC}$ cause a further increase of fuel consumption leading to an overall 13.9% difference with respect to PF-MILP. Once the influence of reserve constraints and forecast errors has been underlined and isolated, the performances of the EMS_{sMPC} (14.4% gap relating to PF-MILP) can be better explained: indeed, its solution approaches the one of $EMS_{PF\text{-}MPC}$ (0.5% difference in fuel consumption), which represents the best results achievable by a perfect second layer. It is worth noticing that, even though EMS_{PI} leads to a 3.3% gap with respect to $EMS_{PF\text{-}MPC}$, its performance is still satisfactory given the non-predictive formulation. On the other hand, lowering the 4.8% difference between $EMS_{PF\text{-}MPC}$ and PF-EMS would require a solution of the first-layer scheduling problem with very accurate forecast throughout the whole optimization horizon, not usually possible in real operation.

6. Conclusions

This paper presents a two-layer hierarchical EMS for the optimal management of multi-goods microgrids under demands and RES generation uncertainty. While the first layer is based on state-of-the-art deterministic MILP model with spinning reserve constraints to compute the optimal unit commitment, a strong focus is given to the second layer problem. The proposed algorithm is formulated as a scenario-based stochastic model predictive control (EMS_{sMPC}). The main features are (i) the introduction of affine piecewise recourse on future disturbances (*i.e.,* forecast errors of net good demands), (ii) the capability of on-line implementation through optimized coefficients for power sharing in the microgrid, and (iii) the mathematical formulation for the proper modelling of BESS with non-simultaneous charge and discharge. An EMS with a PI-based second layer is also considered (EMS_{PI}) as reference case. Both algorithms are conceived for on-field deployment, employing an external workstation to solve the MILP problems, and industrial PLC that receives the schedule and the dispatch rules from the workstation and manages the units in real-time. The implementation was carried out in the Multi-Goods MicroGrid Laboratory of Politecnico di Milano, showing the capability of the EMS to correctly manage an off-grid microgrid that satisfies the demand of electricity and potable water, for several hours of operation and under different PV yields. The experimental activities validated numerical simulation of the EMS, with high accuracy, but some important aspects must be considered:

- SOC estimation plays a crucial role when performing rolling horizon scheduling, as even slight SOC variation between experimental and simulation can lead to different unit commitment, even though the total number of hours of the programmable generator is consistent between the two.
- Non-linear efficiency curves have been used for SOC estimation, but a mismatch can still be observed, due to the working principle of the BMS, that updated the BESS status through voltage measurements of all the cells.
- The average advantage corresponds to 1.7% fuel savings with maximum equal to 3.4%.

Once the two EMS were validated, their performances have been numerically evaluated on a real test case. Assuming the same commitment, the proposed algorithm reduces the fuel costs by 2.7% with respect to PI controller. In addition, it has been demonstrated that it approaches the best possible outcome acting only on the second layer (0.5% gap). The difference between the performances of EMS_{PI} and EMS_{sMPC} is produced by the presence of the wind generator, that causes the uncertainty to spread throughout the day. For MG with only PV systems as RES, the uncertainty is concentrated in few hours during the day (that diminish if the PV fields operate in RPPT), reducing the margin of improvement that EMS_{sMPC} could exploit in optimizing the dispatch. Besides improving forecast accuracy, a further cost reduction can be achieved acting on the first layer model. Future work will consider the development of stochastic first layer formulation, that allow to reduce the over-commitment of dispatchable generators that was noticed in the numerical simulations, mainly due to spinning reserve requirements. Moreover, new interaction paradigms between first and second layer will be considered.

Author statement

Simone Polimeni: Conceptualization, Data curation, Methodology, Software, Validation, Writing original draft. **Lorenzo Meraldi:** Software, Validation. **Luca Moretti:** Conceptualization, Methodology, Writing- review. **Sonia Leva:** Writing- review and editing, Funding Acquisition. **Giampaolo Manzolini:** Conceptualization, Writing-review and editing, Supervision, Funding Acquisition.

Declaration of competing interests

The authors declare that they have no known competing financial interests or personal relationships that could have appeared to influence the work reported in this paper.

Appendix

This section reports the detailed first-layer model, which is a deterministic MILP based predictive optimization with spinning reserve constraints on the various goods' demands.

$$Obj = \sum_{t=1}^{T}\left[\sum_{i}\left(c_{i,t}^{f} + c_{i,t}^{O\&M} + c_{i,t}^{dev}\right) + \sum_{gd}\left(c_{gd,t}^{UM} + c_{gd,t}^{Curt}\right) + c_{i,t}^{SOCdev}\right]\Delta t; \tag{A.1}$$

Where:

$$c_{i,t}^{f} = \hat{k}_{f,t}^{i}\left(\hat{m}_{f}^{i}U_{t}^{i} + \hat{q}_{f}^{i}Z_{t}^{i}\right)\Delta t + \hat{k}_{SU,t}^{i}SU_{t}^{i} = \hat{k}_{f,t}I_{t}^{i}\Delta t + \hat{k}_{SU,t}^{i}SU_{t}^{i}; \quad \forall i \in g_{f}, t \tag{A.2}$$

$$c_{i,t}^{O\&M} = \hat{k}_{O\&M,t}^{i}Z_{t}^{i}\Delta t; \quad \forall i \in g, t \tag{A.3}$$

$$c_{i,t}^{O\&M} = \hat{k}_{O\&M,t}^{i}U_{t}^{s,dh}\Delta t; \quad \forall i \in s, t \tag{A.4}$$

$$c_{gd,t}^{UM} = \hat{k}_{UM,t}^{gd}UM_{t}^{gd}\Delta t;\ c_{gd,t}^{CU} = \hat{k}_{CU,t}^{gd}CU_{t}^{gd}\Delta t; \quad \forall gd, t \tag{A.5}$$

$$c_{i,t}^{SOCdev} = k_{t}^{dev}\Delta_{t}^{SOC} \quad \forall t \tag{A.6}$$

$$\Delta_{t}^{SOC} \geq C_{t}^{BESS1} - C_{t}^{BESS2};\ \Delta_{t}^{SOC} \geq C_{t}^{BESS2} - C_{t}^{BESS1} \quad \forall t \tag{A.7}$$

Programmable generators constraints

$$Z_{t}^{g}, SU_{t}^{g}, SD_{t}^{g} \in \{0,1\} \quad \forall g, t \tag{A.8}$$

$$SU_{t}^{g} \geq Z_{t}^{g} - Z_{t-1}^{g} \quad \forall g, t \tag{A.9}$$

$$SU_{t}^{g} - SD_{t}^{g} = Z_{t}^{g} - Z_{t-1}^{g} \quad \forall g, t \tag{A.10}$$

$$Z_{t}^{g} \geq \sum_{\tau=t}^{\min\left(t+\widehat{UT}^{g},T\right)} SU_{t}^{g} \quad \forall g, t \tag{A.11}$$

$$1 - Z_{t}^{g} \geq \sum_{\tau=t}^{\min\left(t+\widehat{DT}^{g},T\right)} SD_{t}^{g} \quad \forall g, t \tag{A.12}$$

$$I_{t}^{g} = \hat{m}^{g}U_{t}^{g} + \hat{q}^{g}Z_{t}^{g} \quad \forall g, t \tag{A.13}$$

$$\hat{U}_{min}^{g}Z_{t}^{g} \leq U_{t}^{g} \leq \hat{U}_{max}^{g}Z_{t}^{g}; \quad \forall g, t \tag{A.14}$$

$$U_{t}^{g} - U_{t-1}^{g} \leq \widehat{\Delta U}_{UP}^{i} + \widehat{\Delta U}_{max,SU}^{g}SU_{t}^{g}; \quad \forall g, t \tag{A.15}$$

$$U_{t-1}^{g} - U_{t}^{g} \leq \widehat{\Delta U}_{DW}^{i} + \widehat{\Delta U}_{max,SD}^{g}SD_{t}^{g}; \quad \forall g, t \tag{A.16}$$

Storage systems constraints

$$\hat{C}_{min}^{s} \leq C_{t}^{s} \leq \hat{C}_{max}^{s}; \quad \forall s, t \tag{A.17}$$

$$0 \leq U_{t}^{s,dh} \leq \hat{U}_{max}^{s}; \quad \hat{U}_{min}^{s} \leq U_{t}^{s,ch} \leq 0; \quad \forall\ s \notin s^{NS}, t \tag{A.18}$$

$$0 \leq U_{t}^{s,dh} \leq Z_{t}^{s}\hat{U}_{max}^{s};\ \hat{U}_{min}^{s}\left(1 - Z_{t}^{s}\right) \leq U_{t}^{s,ch} \leq 0;\ Z_{t}^{s} \in \{0,1\} \quad \forall\ s \in s^{NS}, t \tag{A.19}$$

$$U_{t}^{s} = U_{t}^{s,dh} + U_{t}^{s,ch}; \quad \forall\ s, t \tag{A.20}$$

$$C_{t+1}^{s} = C_{t}^{s} - \left(\frac{U_{t}^{s,dh}}{\hat{\eta}_{dh}^{s}} + \hat{\eta}_{ch}^{s}U_{t}^{s,ch}\right)\Delta t - \hat{L}^{s}\Delta t; \quad \forall s, t \tag{A.21}$$

Spinning reserve constraints and good balance

$$\sum_{g \in g_{gd}^{pr}} R_{t}^{g} + \sum_{s \in s_{gd}} R_{t}^{s} \geq \left(1 + \Delta\hat{D}_{t,\%}^{gd}\right)\hat{D}_{t}^{gd} + \sum_{g \in g_{gd}^{cn}} U_{t}^{g} \quad \forall gd, t \tag{A.22}$$

$$R_{t}^{g} \leq \hat{U}_{max}^{g}Z_{t}^{g};\ R_{t}^{g} \leq U_{t}^{g} + \widehat{\Delta U}_{UP}^{g}; \quad \forall g \in g_{gd}^{pr}, gd, t \tag{A.23}$$

$$R_{t}^{s} \leq \hat{U}_{max}^{s}; \quad \forall s \in s_{gd}, gd, t \tag{A.24}$$

$$\sum_{\tau=t}^{\min\left(t+\Delta t_{RES},T\right)} R_{t}^{s}\Delta t \leq C_{t}^{s} - \hat{C}_{min}^{s}; \quad \forall s \in s_{gd}, gd, t \tag{A.25}$$

$$\sum_{g \in g_{gd}^{pr}} U_{t}^{g} - \sum_{g \in g_{gd}^{cn}} U_{t}^{g} + \sum_{s \in s_{gd}} U_{t}^{s} + UM_{t}^{gd} = \hat{D}_{t}^{gd} + CU_{t}^{gd}; \quad \forall gd, t \tag{A.26}$$

$$UM_{t}^{gd},\ CU_{t}^{gd} \geq 0 \quad \forall gd, t \tag{A.27}$$

References

[1] Hatziargyriou N, Asano H, Iravani R, Marnay C. Microgrids. IEEE Power Energy Mag Jul-2007;5(4):78–94.
[2] Mancarella P. MES (multi-energy systems): an overview of concepts and evaluation models. Energy 01-Feb-2014;65:1–17 Elsevier Ltd.
[3] Khodaei H, Hajiali M, Darvishan A, Sepehr M, Ghadimi N. Fuzzy-based heat and power hub models for cost-emission operation of an industrial consumer using compromise programming. Appl Therm Eng Jun. 2018;137:395–405.
[4] Zia MF, Elbouchikhi E, Benbouzid M. Microgrids energy management systems: a critical review on methods, solutions, and prospects. Appl Energy Jul. 2018;222:1033–55.
[5] Meng L, Sanseverino ER, Luna A, Dragicevic T, Vasquez JC, Guerrero JM. Microgrid supervisory controllers and energy management systems: a literature review. Renew Sustain Energy Rev 2016;60:1263–73.
[6] Bordons C, Garcia-Torres F, Ridao MA. Model predictive control of microgrids. Springer International Publishing; 2019.
[7] Sen S, Kumar V. Microgrid control: a comprehensive survey. Annu Rev Control 2018;45:118–51.
[8] Olivares DE, et al. Trends in microgrid control. IEEE Trans Smart Grid 2014;5(4).
[9] Luna AC, Diaz NL, Graells M, Vasquez JC, Guerrero JM. Mixed-integer-linear-programming-based energy management system for Hybrid PV-wind-battery microgrids: modeling, design, and experimental verification. IEEE Trans Power Electron Apr. 2017;32(4):2769–83.
[10] Safdarian F, Kargarian A, Kargarian A. Temporal decomposition-based stochastic economic dispatch for smart grid energy management. IEEE Trans Smart Grid Sep. 2020;11(5):4544–54.
[11] Mohammadi S, Soleymani S, Mozafari B. Scenario-based stochastic operation management of MicroGrid including wind, photovoltaic, micro-turbine, fuel cell and energy storage devices. Int J Electr Power Energy Syst Jan. 2014;54:525–35.
[12] Khan AAhmad, Naeem M, Iqbal M, Qaisar S, Anpalagan A. A compendium of optimization objectives, constraints, tools and algorithms for energy management in microgrids. Renew Sustain Energy Rev May 2016;58:1664–83.
[13] Olivares DE, Lara JD, Canizares CA, Kazerani M. Stochastic-predictive energy management system for isolated Microgrids. IEEE Trans Smart Grid Nov. 2015;6(6):2681–93.
[14] Birge JR, Louveaux F. Introduction to stochastic programming. New York, NY: Springer New York; 2011.
[15] Saeedi M, Moradi M, Hosseini M, Emamifar A, Ghadimi N. Robust optimization based optimal chiller loading under cooling demand uncertainty. Appl Therm Eng Feb. 2019;148:1081–91.
[16] Moretti L, Martelli E, Manzolini G. An efficient robust optimization model for the unit commitment and dispatch of multi-energy systems and microgrids. Appl Energy Mar. 2020;261:113859.
[17] Blanco I, Morales JM. An efficient robust solution to the two-stage stochastic unit commitment problem. IEEE Trans Power Syst Nov. 2017;32(6):4477–88.
[18] Abedinia O, Zareinejad M, Doranehgard MH, Fathi G, Ghadimi N. Optimal offering and bidding strategies of renewable energy based large consumer using a novel hybrid robust-stochastic approach. J Clean Prod Apr. 2019;215:878–89.
[19] Lara JD, Olivares DE, Cañizares CA. Robust energy management of isolated microgrids. IEEE Syst J Mar. 2019;13(1):680–91.
[20] Zakaria A, Ismail FB, Lipu MSH, Hannan MA. Uncertainty models for stochastic optimization in renewable energy applications. Renew Energy 01-Jan-2020;145:1543–71 Elsevier Ltd.
[21] Moretti L, Polimeni S, Meraldi L, Raboni P, Leva S, Manzolini G. Assessing the impact of a two-layer predictive dispatch algorithm on design and operation of off-grid hybrid microgrids. Renew Energy Dec. 2019;143:1439–53.

[22] Polimeni S, Moretti L, Manzolini G, Leva S, Meraldi L, Raboni P. Numerical and experimental testing of predictive EMS algorithms for PV-BESS residential microgrid. In: Proc. 2019 IEEE Milan PowerTech; 2019. p. 1–6.
[23] Mesbah A. Stochastic model predictive control: An overview and perspectives for future research. IEEE Control Syst 01-Dec-2016;36(6):30–44 Institute of Electrical and Electronics Engineers Inc..
[24] Oldewurtel F, Jones CN, Parisio A, Morari M. Stochastic model predictive control for building climate control. IEEE Trans Control Syst Technol 2014;22(3):1198–205.
[25] Hans CA, Sopasakis P, Bemporad A, Raisch J, Reincke-Collon C. Scenario-based model predictive operation control of islanded microgrids. In: 2015 54th IEEE Conference on Decision and Control (CDC); 2015. p. 3272–7.
[26] Velarde P, Valverde L, Maestre JM, Ocampo-Martinez C, Bordons C. On the comparison of stochastic model predictive control strategies applied to a hydrogen-based microgrid. J Power Sources 2017;343:161–73.
[27] Elkazaz M, Sumner M, Naghiyev E, Pholboon S, Davies R, Thomas D. A hierarchical two-stage energy management for a home microgrid using model predictive and real-time controllers. Appl Energy Jul. 2020;269:115118.
[28] Valibeygi A, konakalla sai akhil reddy, de Callafon R. Predictive hierarchical control of power flow in large-scale PV Microgrids with energy storage. IEEE Trans Sustain Energy Jun. 2020 1–1.
[29] Raimondi Cominesi S, Farina M, Giulioni L, Picasso B, Scattolini R. A two-layer stochastic model predictive control scheme for Microgrids. IEEE TransControl Syst Technol Jan. 2018;26(1):1–13.
[30] Kou P, Feng Y, Liang D, Gao L. A model predictive control approach for matching uncertain wind generation with PEV charging demand in a microgrid. Int J Electr Power Energy Syst Feb. 2019;105:488–99.
[31] Zhang Y, Meng F, Wang R, Kazemtabrizi B, Shi J. Uncertainty-resistant stochastic MPC approach for optimal operation of CHP microgrid. Energy Jul. 2019;179:1265–78.
[32] Zhang Y, Meng F, Wang R, Zhu W, Zeng X-J. A stochastic MPC based approach to integrated energy management in microgrids. Sustain. Cities Soc. Aug. 2018;41:349–62.
[33] Safdarian F, Kargarian A. Time decomposition strategy for securityconstrained economic dispatch. IET Gener Transm Distrib Nov. 2019;13(22):5129–38.
[34] Elma O, Taşcıkaraoğlu A, Tahir İnce A, Selamoğulları US. Implementation of a dynamic energy management system using real time pricing and local renewable energy generation forecasts. Energy Sep. 2017;134:206–20.
[35] Elsied M, Oukaour A, Youssef T, Gualous H, Mohammed O. An advanced real time energy management system for microgrids. Energy Nov. 2016;114:742–52.
[36] Elkazaz M, Sumner M, Thomas D. Energy management system for hybrid PV-wind–battery microgrid using convex programming, model predictive and rolling horizon predictive control with experimental validation. Int J Electr Power Energy Syst Feb. 2020;115:105483.
[37] Hooshmand A, Asghari B, Sharma RK. Experimental demonstration of a tiered power management system for economic operation of grid-tied microgrids. IEEE Trans Sustain Energy Oct. 2014;5(4):1319–27.
[38] Parisio A, Rikos E, Glielmo L. Stochastic model predictive control for economic/environmental operation management of microgrids: an experimental case study. J. Process Control 2016;43:24–37.
[39] Wu J, Xing X, Liu X, Guerrero JM, Chen Z. Energy management strategy for grid-tied microgrids considering the energy storage efficiency. IEEE Trans Ind Electron Dec. 2018;65(12):9539–49.
[40] Luna AC, Meng L, Diaz NL, Graells M, Vasquez JC, Guerrero JM. Online energy management systems for microgrids: experimental validation and assessment framework. IEEE Trans Power Electron Mar. 2018;33(3):2201–15.
[41] "Multi-goods Microgrid laboratory." [Online]. Available: https://www.mg2lab.polimi.it/.
[42] Shi W, Li N, Chu CC, Gadh R. Real-time energy management in Microgrids. IEEE Trans Smart Grid Jan. 2017;8(1):228–38.
[43] Camacho EF, Bordons C. Introduction to model predictive control. In: Advanced textbooks in control and signal processing. Springer International Publishing; 2007. p. 1–11. no. 9781852336943.
[44] Raković SV, Levine WS, editors. Handbook of model predictive control. Cham: Springer International Publishing; 2019.
[45] Astolfi M, Mazzola S, Silva P, Macchi E. A synergic integration of desalination and solar energy systems in stand-alone microgrids. Desalination Oct. 2017;419:169–80.
[46] G. E. P. Box, G. M. Jenkins, and G. C. Reinsel, *Time series analysis forecasting and control*, John Wiley.
[47] Raza MQ, Nadarajah M, Ekanayake C. On recent advances in PV output power forecast. Solar Energy 15-Oct-2016;136:125–44 Elsevier Ltd.
[48] Nespoli A, Mussetta M, Ogliari E, Leva S, Fernández-Ramírez L, García-Triviño P. Robust 24 hours ahead forecast in a Microgrid: a real case study. Electronics Dec. 2019;8(12):1434.
[49] Gröwe-Kuska N, Heitsch H, Römisch W. Scenario reduction and scenario tree construction for power management problems. In: 2003 IEEE Bologna PowerTech - Conference Proceedings, 3; 2003. p. 152–8.
[50] Lofberg J. YALMIP : a toolbox for modeling and optimization in MATLAB. In: 2004 IEEE International Conference on Robotics and Automation (IEEE Cat. No.04CH37508); 2004. p. 284–9.
[51] Guorobi Optimization L. Gurobi optimizer reference manual; 2018. [Online]. Available: http://www.gurobi.com.
[52] Rigovacca O, Polimeni S, Manzolini G, Leva S, Raboni P. Analyses of electrification and battery ageing processes in a real Offgrid hybrid Microgrid. In: Proc. 2019 IEEE Milan PowerTech; 2019. p. 1–6.
[53] N. R. E. L. Xiangkun Li, N. R. E. L. James Salasovich, and N. R. E. L. Tim Reber, "Microgrid load and LCOE modelling results | NREL data catalog." [Online]. Available: https://data.nrel.gov/submissions/79.
[54] Dolara A, Leva S, Manzolini G. Comparison of different physical models for PV power output prediction. Sol Energy Sep. 2015;119:83–99.